Title page

Title: High-altitude hypoxia exposure inhibits erythrophagocytosis by inducing macrophage ferroptosis in the spleen

Running title: Hypobaric hypoxia induces splenic ferroptosis

Type of article: Research article

Authors: *Wan-ping Yang*[1△], *Mei-qi Li*[1△], *Jie Ding*[1], *Jia-yan Li*[1], *Gang Wu*[2,3], *Bao Liu*[2,3], *Yu-qi Gao*[2,3], *Guo-hua Wang*[1,4]*, *Qian-qian Luo*[1]*

[△]These authors contributed equally to this work.

Affiliations:

[1]Department of Physiology and Hypoxic Biomedicine, Institute of Special Environmental Medicine and Co-innovation Center of Neuroregeneration, Nantong University, 9 Seyuan Road, Chongchuan District, Nantong, Jiangsu 226019, China.

[2]College of High-Altitude Military Medicine, Institute of Medicine and Hygienic Equipment for High Altitude Region, Army Medical University, Chongqing 400038, China.

[3]Key Laboratory of Extreme Environmental Medicine and High-Altitude Medicine, Ministry of Education of China, Chongqing 400038, China.

[4]Department of Neurosurgery, Southwest Hospital, Army Medical University, Chongqing, Chongqing 400038, China

*Corresponding author: Guohua Wang, Email-address: wgh036@hotmail.com, ORCID: 0000-0002-4810-8534; or Qianqian Luo, Email-address: qianqianluo@ntu.edu.cn , ORCID: 0000-0001-8302-3117.

Abstract

High-altitude polycythemia (HAPC) is a chronic condition prevalent in individuals residing at high altitudes (HA), characterized by an augmented production of red blood cells (RBCs) due to hypoxic conditions. Despite its prevalence, the pathophysiological basis and molecular mechanisms driving HAPC remain largely unelucidated. In our study, we utilized a mouse model exposed to hypobaric hypoxia (HH), replicating the environmental conditions experienced at 6000 m above sea level, coupled with *in vitro* analysis of primary splenic macrophages under 1% O_2 to investigate these mechanisms. Our findings revealed that HH exposure significantly stimulates erythropoiesis, leading to erythrocytosis. This was accompanied by a notable sequence of splenic changes, initially characterized by splenic contraction, which subsequently progressed to splenomegaly over 14 days. A key observation was the impairment on the capacity of spleen to process RBCs, primarily attributed to a reduction in splenic macrophages located in the red pulp. Extended HH treatment over 7 and 14 days precipitated increased iron mobilization and the onset of ferroptosis within the spleen. This was evidenced by altered expression levels of iron metabolism and ferroptosis-related proteins, paralleling gene expression patterns observed in human peripheral blood mononuclear cells. Single-cell sequencing of splenic tissue post-HH exposure demonstrated a marked decrease in macrophage populations after 7 days. Our study further disclosed a significant increase in RBCs retention in the spleen following HH exposure, likely a consequence of diminished red pulp macrophages (RPMs) and erythrophagocytosis. This hypothesis was

corroborated through comprehensive analyses involving flow cytometry, histological staining, and immunostaining, which collectively provided a detailed understanding of RBCs dynamics under HH conditions. *In vitro* analyses substantiated the decline in primary splenic macrophages and induction of ferroptosis under hypoxic treatment, effects that were relieved by pre-treatment with the ferroptosis inhibitor ferrostatin-1. Collectively, our data suggest that HH exposure initiates splenic ferroptosis, leading primarily to a decrease in RPMs. This decrease potentially impacts erythrophagocytosis, contributing to increased RBCs retention and subsequent splenomegaly. Such changes could potentially foster continuous RBCs production and accelerate the progress of HAPC. In conclusion, our study highlights the important role of the spleen and splenic macrophages in the pathogenesis of HAPC, providing crucial insights into the disease progression and potential therapeutic targets.

Keywords: High altitude, Hypobaric hypoxia, High-altitude polycythemia, Spleen, Macrophage, Erythrophagocytosis, Ferroptosis

Background

A plateau is a special environment characterized by low atmospheric pressure and low partial oxygen pressure. Long-term exposure to plateau environments may lead to chronic mountain disease [1]. High-altitude polycythemia (HAPC) is a common and widespread chronic mountain sickness characterized by excessive erythrocytosis [2]. Hypobaric hypoxia (HH) is the main cause of erythrocytosis, which in turn alleviates hypoxic conditions in tissues under high-altitude (HA) exposure [3]. In a healthy

organism, a balance is maintained between erythropoiesis in the bone marrow (BM) and erythrophagocytosis in the spleen [4]. Even though HA/HH exposure can disrupt the equilibrium between RBCs formation and clearance, healthy individuals can swiftly establish a new steady state of RBCs homeostasis in chronic hypoxia [5]. This adaptation is a critical response to the altered oxygen availability characteristic of HA environments. However, in patients with HAPC, RBCs homeostasis is disrupted, failing to reach a state of equilibrium, which ultimately leads to a persistent increase in RBCs count [4]. This deviation from the normative adaptation process implies a pathological deviation from the usual compensatory mechanisms employed under chronic hypoxia conditions [6]. It is well-established that exposure to HA/HH can induce erythropoiesis, yet the pathogenesis of erythrophagocytosis under these conditions remains poorly understood [7].

The spleen plays a crucial role in maintaining erythropoietic homeostasis by effectively clearing impaired and senescent RBCs from circulation [8]. Particularly, red pulp macrophages (RPMs) within the spleen, serving as primary phagocytes, are responsible for clearing senescent, damaged, and abnormal erythrocytes from circulation to recycle iron [9]. RPMs initiate the process of RBCs endocytosis and lysosomal digestion into heme, following the recognition of the RBCs earmarked for removal via their cell surface signals [10, 11]. Subsequently, heme oxygenase-1 (HO-1) decomposes the heme into biliverdin, carbon monoxide, and iron [12]. Most of the iron recycled from heme is transported out of the cell through a protein called ferroportin (Fpn). This iron then binds to transferrin (Tf), a plasma protein that

transports iron in the blood. The iron-transferrin complex interacts with the transferrin receptor (TfR) on the cell membrane, contributing to the formation of RBCs in the erythroid compartment [13]. A portion of the released iron is loaded into cellular ferritin (Ft; including Ft-H and Ft-L). In the presence of oxygen, the Ft-H facilitates the oxidation of Fe^{2+} (ferrous ion) to Fe^{3+} (ferric ion). Subsequently, the Ft-L stores this Fe^{3+} [14]. The Ft-L features a nucleation site, consisting of a cluster of cavity-exposed carboxyl residues, which readily bind to Fe^{3+}, thereby simplifying the storage process [15]. When the iron metabolism is vigorous, nuclear receptor coactivator 4 (NCOA4) can recognize Ft-H, bring Ft into the lysosomal pathway for degradation, and release iron in Ft for iron utilization in the body [16]. However, some iron exists in cells in the form of ferrous iron (Fe^{2+}), which is well known to be an important initiator of free radical oxidation [6]. Moreover, the accumulation of large amounts of Fe^{2+} in cells may cause ferroptosis [17].

Despite the extensive study of erythropoiesis under HA/HH conditions, the precise effects of HA/HH on erythrophagocytosis within the spleen remain largely unexplored. Considering the significant role of the spleen in RBC processing and the crucial function of RPMs in iron recycling from RBC clearance, we evaluated the impacts of HA exposure on the spleen/splenic macrophages using an HH-exposed mouse model (simulating 6000 m exposure conditions). In the current study, we sought to further investigate whether HA/HH can influence the erythrocyte disposal and iron recycling processes in macrophages. More specifically, we aimed to determine the potential impact of HA/HH exposure on the integrity of the

erythrophagocytosis process. We discovered that exposure to HH triggered ferroptosis in the spleen, particularly in macrophages. This led to a reduction in macrophage numbers, which was subsequently followed by disruptions in erythrophagocytosis and iron recycling within the spleen. These findings may hold clinical significance, particularly in the context of continuous pathological erythrocytosis and the progression of HAPC under HA exposure.

Methods

HH mouse exposure model

Male C57BL/6 male mice (at 8 weeks of age) were obtained from the animal experimental centre of Nantong University. Mice were adapted to the facilities for 3 days before experiments. Mouse models of HH exposure were established by placing the mice in the decompression chamber (TOW-INT TECH, ProOx-810, China) for 1, 2, 3, 7, and 14 days. The parameters were set as follows: 6000 m above sea level, oxygen partial pressure of 11 kPa, lifting speed of 20 m/s, chamber pressure of 54 kPa, temperature of 25 °C, humidity of 40%, and 12-h light/dark cycles. The hypobaric chamber was configured to ensure a ventilation rate of 25 air exchanges per minute. Tuftsin (0.15 mg/kg, MCE, HY-P0240, USA) was used to stimulate the phagocytosis of macrophages [18], and was injected at 7 and 11 days during the 14-days period of mice exposed to HH. The control group animals were maintained in a similar chamber for the same amount of time under normobaric normoxia (NN) conditions.

Splenectomy

After anesthesia, the mice were placed in a supine position, and their limbs were fixed. The abdominal operation area was skinned, disinfected, and covered with a sterile towel. A median incision was made in the upper abdomen, followed by laparotomy to locate the spleen. The spleen was then carefully pulled out through the incision. The arterial and venous directions in the splenic pedicle were examined, and two vascular forceps were used to clamp all the tissue in the main cadre of blood vessels below the splenic portal. The splenic pedicle was cut between the forceps to remove the spleen. The end of the proximal hepatic artery was clamped with a vascular clamp, and double or through ligation was performed to secure the site. The abdominal cavity was then cleaned to ensure there was no bleeding at the ligation site, and the incision was closed. Post-operatively, the animals were housed individually. Generally, they were able to feed themselves after recovering from anesthesia and did not require special care.

Splenic macrophage culture and treatments

After isoflurane anaesthesia, mice were transcardially perfused with precooled PBS, and then splenic tissue was collected. The spleen was then dissected into minuscule fragments, each approximately 1 mm^3 in volume, and separated in cold, phenol red-free Hanks' balanced salt solution (HBSS; Gibco, Grand Island, NY, USA). The cell extracts were centrifuged at 500 rpm for 5 min at 4 °C. The pellets were then resuspended and incubated with ammonium-chloride-potassium (ACK) lysing buffer (Thermo Fisher Scientific, USA) for 3 min at room temperature. Next, cell extracts

were purified in a four-phase Percoll (Sigma–Aldrich, St. Louis, MO, USA) gradient: 0, 30, 40, and 50% in HBSS. After centrifugation at 500 rpm for 20 min at 4°C, the macrophage-enriched fraction was collected at the interface between the 30% and 40% phases. Cells were washed in two rounds with HBSS and then resuspended in AIM V medium (Thermo Fisher Scientific). The cells in this medium were cultured at 37 ℃ and 5% CO_2 for 12 h. After the cells were treated with ferrostatin-1 (Fer-1, 2 μm; Selleck Chemicals, S7243, USA) 1 h in advance, the cells were placed in a hypoxia workstation (Invivo2, Ruskinn, UK) for 24 h.

Blood smear and hematological indices

The collected blood was gently mixed with EDTA (15 g/L) to obtain anticoagulant blood, which was detected by a hematology analyser (XE-5000, Sysmex Corporation, Japan). Blood smear preparation method: a blood sample is dropped onto a slide, and another slide is used to push the blood sample into a uniform thin layer at a constant speed. After the blood samples were dried, Wright stain solution (G1040, Solarbio, China) was added and incubated for 1 min. Then, the slide was rinsed with water. Blood smears were photographed with a DM4000B microscope (Leica, Germany).

Lillie staining and Hematoxylin and Eosin (HE) staining

The Lillie staining method was employed to ascertain Fe^{2+} deposition within the spleen, according to the protocol delineated by Liu et al [19]. Briefly, paraffin-embedded spleen sections underwent a process of dewaxing and rehydration

via xylene and gradient alcohol. Then, the Lillie staining solution (G3320, Solarbio, China) was applied at 37°C for 50 min in a light-restricted environment, improved by a 5-min PBS wash. Subsequently, a mixture comprising 30% hydrogen peroxide and methanol was incubated for 20 min, and then the sections were subjected to two 5-min washes with PBS. The DAB developing solution, which is not included in the Lillie bivalent iron staining kit, was applied for light-sensitive staining. The sections were stained with a nuclear fast red solution in a light-restricted setting for 10 min, followed by a 5-second wash with ddH_2O. Lastly, the sections were dehydrated with gradient alcohol, cleared with xylene, and mounted with neutral resin. HE staining was employed in the spleen according to our previous study [20].

Wright-Giemsa composite stain

Mice were anaesthetized and perfused with saline. The spleen was subsequently excised to prepare a single cell suspension, achieved by filtering through a 70 μm filter. Samples were centrifuged at 500 g for 5 min for cell separation. The cell pellet was subjected to three PBS washes. The suspension was then smeared onto a slide and air-dried. Following this, the slide was stained with Wright-Giemsa composite stain (G1020, Solarbio, China) for 3 min. An equivalent volume of pH 6.4 phosphate buffer was introduced, and the slide was gently agitated to allow mixing with the Wright's stain solution for 5 min. After washing and drying, a microscope (DM4000B, Leica, Germany) was utilized for visualization and image acquisition.

Western blot

Tissue and cell samples were homogenized on ice after cell lysates and protease inhibitors were added. Centrifugation was performed at 12,000 rpm for 15 min at 4°C to collect the supernatant. Protein concentration was determined by the BCA detection method. A sample containing 30 μg protein was loaded and run in each well of SDS–PAGE gels. The membranes were incubated with the following antibodies: HO-1 (1:2000, Abcam, ab13243, USA); Ft-L (1:1000, Abcam, ab69090, USA); Ft-H (1:1000, Novus, NBP1-31944, USA); NCOA4 (1:1000, Santa Cruz, sc-373739, USA); TfR (1:1000, Thermo Fisher, 13-6800, USA); Fpn (1:1000, Novus, NBP1-21502, USA); ACSL4 (1:1000, Santa Cruz, sc-271800, USA); xCT (1:1000, Proteintech, 26864-1-AP, USA); Gpx4 (1:1000, Abcam, ab125066, USA); CD206 (1:1000, RD, AF2535, USA); and β-actin (1:1000, Sigma–Aldrich, A5316, USA). The secondary antibodies were as follows: goat anti-mouse (1:10000, Jackson, USA) and goat anti-rabbit (1:10000, Jackson, USA). The gray value of specific blots was scanned and analysed using ImageJ software (National Institute of Health, USA).

RT–PCR analysis

Total RNA extraction and RT–PCR analysis were performed essentially as described previously [21]. Primer sequences were as follows:

Gene	Primer sequence (5’-3’)	Product length (bp)
Csf1	F: GGCTTGGCTTGGGATGATTCT R: GAGGGTCTGGCAGGTACTC	126
Csf2	F: GGCCTTGGAAGCATGTAGAGG R: GGAGAACTCGTTAGAGACGACTT	104
CCL2	F: TTAAAAACCTGGATCGGAACCAA	121

	R: GCATTAGCTTCAGATTTACGGGT	
CCL7	F: GCTGCTTTCAGCATCCAAGTG	135
	R: CCAGGGACACCGACTACTG	

GEO analysis

GSE46480 samples were found in the GEO database of NCBI with the keyword "High Altitude" search. The data set was divided into two groups, one for the plain (Base Camp) and the other for the plateau (Altitude), with a sample size of 98 for each group. Blood samples were collected from the same person at McMurdo Station (48 m) and immediately transferred to Amundsen-Scott South Pole Station (2835 m) on the third day. R language was used for data analysis, and GraphPad Prism was used for statistics.

Malondialdehyde (MDA), Cysteine (Cys) and Glutathione (GSH) content detection

MDA was detected by a Micro Malondialdehyde Assay Kit (Solarbio, BC0025, China). Cys was detected by a Micro Cysteine Assay Kit (Solarbio, BC0185, China). GSH was detected by a Micro Reduced Glutathione Assay Kit (Solarbio, BC1175, China).

Immunofluorescence

Spleen sections of 9 μm thickness were flash-frozen and stored at -80°C. Before immunofluorescence staining, these sections were allowed to acclimate to room temperature for 30 min, then incubated in 10% BSA-PBS for 10 min. Next, the

sections were incubated overnight with F4/80-PE (1:200, Biolegend, 123110, USA) or F4/80 (1:100, ab16911, Abcam, USA) and then washed thrice with PBS. Due to the limitations of F4/80 as a definitive macrophage marker, we concurrently conducted immunohistochemical analysis for heme oxygenase-1 (HO-1) (1:200, Abcam, ab13243, USA), CD11b (1:100, 14-0112-82, Thermo, USA) and CD68 (1:100, ab125212, Abcam, USA), respectively. In the RBCs detection experiment, Band3 primary antibody (1:100, 2813101-AP, Proteintech, China) and PKH67 green fluorescent cell linker (1:250, MIDI67, Sigma, USA) were used. Following this, sections were washed thrice with 0.05% PBST, incubated with secondary antibodies DAR-Alexa555 at room temperature for 2 h, washed thrice with PBS again, and finally sealed with 50% glycerine-PBS. Fluorescence microscopy images were captured using a confocal laser scanning microscope (SP8, Leica Microsystems, Wetzlar, Germany). To quantify the immunostaining intensity of F4/80, HO-1, CD11b, CD68, we utilized ImageJ software. Specifically, we captured multiple fields of view for each slide, and the software was used to measure the mean intensity of the fluorescent signal in these images. These measurements were then normalized to the NN group to account for any experimental variations.

Tissue iron staining (DAB-enhanced Perls' staining)

DAB-enhanced Perls' staining for the spleen paraffin sections was performed as described previously [20]. Briefly, the sections were washed with PBS and cultured in freshly prepared Perls' solution (1% potassium ferricyanide in 0.1 M hydrochloric

acid buffer). The slides were then immersed and stained with DAB. All slides were counterstained with hematoxylin and visualized under a DM4000B microscope (Leica, Germany). Data were collected from three fields of view per mouse and semiquantitatively analysed with ImageJ software. Quantitative results of iron staining were finally normalized to the NN control group.

Flow cytometry

1) The steps of reticulocyte ratio detection were as follows: Whole blood was extracted from the mice and collected into an anticoagulant tube, which was then set aside for subsequent thiazole orange (TO) staining [22]. The experimental tube and negative control tube were prepared, 125 μL normal saline, 4 μL anticoagulant and 125 μL TO working solution (1 μg/mL, Sigma, 390062, USA) were added to each tube, and 250 μL normal saline and 4 μL anticoagulant were added to each tube of the negative control tube. After incubation at room temperature for 1 h, flow cytometry analysis was carried out by using the FL1 (488 nm/525 nm) channel.

2) The steps for the determination of intracellular divalent iron content and lipid peroxidation level were as follows: Splenic tissue was procured from the mice and subsequently processed into a single-cell suspension using a 40 μm filter. The RBCs within the entire sample were subsequently lysed and eliminated, and the remaining cell suspension was resuspended in PBS in preparation for ensuing analyses. A total of 1×10^6 cells were incubated with 100 μL of BioTracker Far-red Labile Fe^{2+} Dye (1 mM, Sigma, SCT037, USA) for 1 h or C11-BODIPY 581/591 (10 μM, Thermo Fisher,

D3861, USA) for 30 min. After the cells were washed with PBS twice, flow cytometry analysis was carried out by using the FL6 (638 nm/660 nm) channel for determination of intracellular divalent iron content or the FL1 (488 nm/525 nm) channel for determination of lipid peroxidation level.

3) The steps for detecting the mortality of spleen cells and macrophages were as follows: 1×10^6 cells were incubated at room temperature for 40 min with 2 μM Calcein AM and 8 μM Propidium Iodide (PI). Flow cytometry analysis was carried out by using FL1 (488 nm/525 nm, Calcein AM) and FL3 (488 nm/620 nm, PI) channels.

4) The steps for detecting the number of RPMs in the spleen were as follows: 1×10^6 cells were incubated with 2% mouse serum-PBS for 10 min, incubated with F4/80-PE (1:1000, 565410, BD, USA) and CD11b PE-CY7 M1/70 (1:1000, 552850, BD, USA) for 30 min, and washed with 2% mouse serum-PBS twice. Flow cytometry analysis was carried out by using FL2 (488 nm/575 nm, F4/80- PE) and FL5 (488 nm/755 nm, CD11b PE-CY7 M1/70) channels.

5) The steps for detecting the number of monocytes in blood, spleen and bone marrow were as follows: 1×10^6 cells were incubated with 2% mouse serum-PBS for 10 min, incubated with F4/80-PE, CD11b-PE/CY7 (1:2000, BD, 552850, USA), and Ly6C-APC (1:2000, Thermo Fisher, 17-5932-82) for 30 min, and washed with 2% mouse serum-PBS twice. Flow cytometry analysis was carried out by using FL2 (488 nm/575 nm, F4/80- PE), FL5 (488 nm/755 nm, CD11b-PE/CY7) and FL6 (638 nm/660 nm, Ly6C-APC) channels.

6) The steps employed for assessing erythrophagocytosis in the spleen was scrupulously performed as follows: Initially, RBCs were harvested from mice and subjected to *in vitro* labelling with PKH67 cell linker. Subsequently, these PKH67-labeled RBCs were administered into mice, followed by exposure to either NN or HH. After a duration of 7 or 14 days of exposure, splenic single-cell suspensions were carefully prepared. From these suspensions, a quantity of 1×10^6 cells was isolated and washed in PBS for a period of 5 min. The analytical phase involved flow cytometry, utilizing the FL1 channel (490 nm excitation/502 nm emission) specifically used for detecting PKH67. This approach facilitated the precise quantification and analysis of erythrophagocytosis within the spleen under the specified experimental conditions.

Phagocytosis of *E. coli* and RBCs

E. coli was labelled with Cy5.5 (5 mg/mL), and RBCs were labelled with NHS-biotin (20 mg/mL). Macrophages (1×10^6) were coincubated with *E. coli*-Cy5.5 or RBC-Biotin for 30 min and washed with 2% mouse serum-PBS twice. Flow cytometry analysis was carried out by using FL6 (638 nm/660 nm) to determine the phagocytosis of spleen by *E. coli*. Macrophages (coincubated with Biotin-RBCs) were incubated with streptavidin-FITC for 3 h and washed twice with 2% mouse serum PBS. FL1 (488 nm/525 nm) was used for flow cytometry analysis to determine the phagocytosis of RBCs in the spleen.

Single-cell RNA Sequencing

The spleen tissues were surgically removed and stored in MACS Tissue Storage Solution (Miltenyi Biotec, Bergisch Gladbach, Germany) until processing. Single-cell dissociation was performed by the experimentalists at the GENECHEM laboratory (Shanghai, China). Dissociated single cells were then stained for viability assessment using Calcein-AM (BD Biosciences, USA) and Draq7 (BD Biosciences). The BD Rhapsody system was used to capture transcriptomic information from single cells. Single-cell capture was achieved by random distribution of a single-cell suspension across >200,000 microwells through a limited dilution approach. Beads with oligonucleotide barcodes were added to saturation so that a bead was paired with a cell in a microwell. The cells were lysed in the microwell to hybridize mRNA molecules to barcoded capture oligos on the beads. Beads were collected into a single tube for reverse transcription and ExoI digestion. Upon cDNA synthesis, each cDNA molecule was tagged on the 5′ end (that is, the 3′ end of an mRNA transcript) with a unique molecular identifier (UMI) and cell barcode indicating its cell of origin. Whole transcriptome libraries were prepared using the BD Rhapsody single-cell whole-transcriptome amplification (WTA) workflow, including random priming and extension (RPE), RPE amplification PCR and WTA index PCR. The libraries were quantified using a High Sensitivity D1000 ScreenTape (Agilent) and High Sensitivity D1000 Reagents (Agilent) on a 4150 TapeStation System (Agilent, Palo Alto, CA, USA) and the Qubit High Sensitivity DNA assay (Thermo Fisher Scientific). Sequencing was performed on an Illumina sequencer (Illumina Nova Seq 6000, San

Diego, CA) in a 150 bp paired-end run.

Statistical analysis

Statistical analysis was conducted using GraphPad Prism 8.0 software. All values were represented as the mean ± standard error (SEM). The homogeneity of variance was verified before the application of a parametric test. A two-tailed Student's t-test was employed for data from two groups, while a one-way analysis of variance (ANOVA) with multiple comparisons using Tukey's post hoc test was utilized for data from multiple groups. A p-value of less than 0.05 was considered statistically significant.

Results

HH exposure promotes erythrocytosis in mice

To mimic 6000 m HA exposure, we placed C58BL/6 mice in an animal hypobaric oxygen chamber and detected the blood indices in the blood of the mice after HH exposure for different times. The blood smear showed that the number of RBCs was increased from 3 to 14 days after HH exposure compared with the NN group (Figure 1A). Routine blood tests further confirmed the results in blood smears, which showed that the RBC number (Figure 1B), HGB content (Figure 1C) and HCT value (Figure 1D) were all increased significantly to varying degrees, while MCH was not changed after HH exposure (Figure 1E). We further performed flow cytometry using TO

staining to detect reticulocytes after 3, 7, and 14 days of HH treatment. The results showed that the proportion of reticulocytes increased after 7 and 14 days of HH exposure (Figure 1, F-G), and the number of RBCs reached the peak after 7 days of HH exposure. These results suggested that the HH-treated mouse model effectively mimics HA exposure, which promotes erythropoiesis and results in erythrocytosis in mice following HH exposure.

Spleen inhibits the immoderate increase in RBCs under HH conditions

To determine the roles of the spleen in RBC homeostasis under HA/HH, we investigated the effects of HH on the morphology, volume, and weight of the spleen as well as erythrocyte indices. As shown in Figure 2, the spleen volume and weight were decreased significantly after HH exposure for 1 day compared to NN treatment (Figure 2, A-C). However, the spleen was obviously enlarged from 2 to 14 days after HH exposure (Figure 2, A-C). The results indicated that the spleen contracted, the stored RBCs in the spleen were released into the blood at 1 day, and the RBCs were produced and/or retained in the spleen from 2 to 14 days after HH exposure. In our research, we also examined the influence of the spleen on RBCs homeostasis under HH conditions. We investigated whether the role of spleen in RBCs clearance under HH conditions could be compensated by the liver or other components of the mononuclear macrophage system. To conduct this, we performed splenectomies on mice and subsequently exposed them to HH conditions for 14 days. This allowed us to monitor RBCs counts and blood deposition. Our findings indicated that, in

comparison to both the splenectomized mice under NN conditions and the sham-operated mice exposed to HH, erythrocyte deposition (Figure 2D) and counts (Figure 2E), as well as HGB (Figure 2F) and HCT (Figure 2G) levels, significantly increased 14 days post-splenectomy under HH conditions. Meanwhile, MCH levels remained stable (Figure 2H). These indices did not vary in mice, regardless of whether they had undergone a splenectomy, under NN conditions (Figure 2D and E). These results indicate that in the splenectomized group under NN conditions, erythrophagocytosis is substantially compensated for by functional macrophages in other tissues. However, under HH conditions, our data also suggest that the spleen plays an important role in managing erythrocyte turnover, as indicated by the significant impact of splenectomy on erythrophagocytosis and subsequent RBCs dynamics.

HH exposure leads to a decrease in splenic macrophages

Considering macrophages as the primary cell type responsible for processing RBCs within the spleen under physiological conditions, we subsequently investigated the population and activity of these macrophages after exposure to HH for 7 or 14 days, employing flow cytometry and single-cell sequencing techniques. Calcein/PI double staining, examined via flow cytometry, revealed a significant decrease in viable splenic cells and a concomitant increase in dead cells following 7 and 14 days of HH exposure (Figure 3, A-C). This observation was further substantiated by single-cell sequencing, which elucidated a pronounced reduction in the population of splenic

macrophages after 7 days of HH exposure (Figure 3, D-F). Additionally, flow cytometry results indicated a marked decrease in the population of RPMs, identified as F4/80^{hi}CD11b^{lo}, in the spleen post 7 days of HH exposure (Figure 3G). Complementary to these findings, immunofluorescence detection demonstrated a significant diminution in RPMs, characterized by F4/80^{hi}CD11b^{lo} and F4/80^{hi}CD68^{hi} cell populations, after both 7 and 14 days of HH exposure (Figure S1). Furthermore, our single-cell sequencing analysis of the spleen under NN conditions revealed a predominant association of RPMs with Cluster 0. Intriguingly, HH exposure led to a notable reduction in the abundance of RPMs within this cluster. Pseudo-time series analysis provided insights into the transitional dynamics of spleen RPMs, indicating a shift from Cluster 2 and Cluster 1 towards Cluster 0 under NN conditions. However, this pattern was altered under HH exposure, where a shift from Cluster 0 and Cluster 1 towards Cluster 2 was observed (Figure S2).

To further elucidate the migration and differentiation of monocytes from the bone marrow to the spleen, we analysed the expression of chemokines CCL2, CCL7, Csf1, and Csf2 in the spleen using qPCR and determined the number of monocytes in the bone marrow (BM) and spleen via flow cytometry. Our results indicated a significant reduction in the expression of CCL2, CCL7 (Figure 3H), Csf1, and Csf2 (Figure 3I) in the spleen after 7 and 14 days of HH exposure. Furthermore, the number of monocytes (Ly6C^{+}/CD11b^{+}) in the bone marrow (Figure 3, J-L) and spleen (Figure 3, J and M-N) also exhibited a decline after 7 and 14 days of HH exposure. We evaluated the depletion of macrophages in the spleen under HH conditions by

examining the expression and distribution of HO-1 and F4/80. There was a decrease in both HO-1 and F4/80, predominantly within the splenic red pulp following HH exposure (Figures 3, O-Q). Together, these findings indicate a reduction in the number of splenic macrophages after HH exposure, which could impair the spleen's capacity to process erythrocytes.

HH exposure suppresses erythrophagocytosis of RPMs in spleen

We investigated the influence of HH exposure on erythrocyte phagocytosis and heme iron recycling within splenic macrophages. To this end, we implemented a dual approach: administering NHS-biotin intravenously to mice, followed by HH exposure, and subsequently introducing PKH67-labelled RBCs into the mice, also followed by HH treatment *in vivo*. This methodology allowed us to monitor the clearance of RBCs by tracking the retention of both biotin-labelled and PKH67-labelled RBCs using flow cytometry in the blood and spleen of the HH-treated mice. Our findings (as detailed in Figure 4) indicated a pronounced decrease in the presence of both biotin-labelled and PKH67-labelled RBCs in the blood and spleen at 7- and 14-day intervals post HH exposure. Notably, while a natural decline in labelled RBCs over time was expected, the rate of decay was significantly more acute in the NN exposure group as compared to the HH group. This observation was consistent across both blood (Figure 4, A and C; Figure 4, E and G) and spleen samples (Figure 4, B and D; Figure 4, F and H). Furthermore, our analysis revealed that the phagocytic capacity of mouse spleen macrophages toward RBCs was notably diminished following HH exposure,

particularly on the 14th day (Figure 4, A-D; Figure 4, E-H). To confirm these findings, we conducted additional assessments of the PKH67-positive RPMs cell population through both flow cytometry and immunofluorescence detection in the spleen post HH exposure. The findings revealed that both the population of splenic RPMs ($F4/80^{hi}CD11b^{lo}$) (Figure 5, A-B) and the PKH67-positive macrophages (Figure 5, A and C; D-E) consistently demonstrated a substantial reduction after 7 or 14 days of HH exposure, further reinforcing the impact of HH on the erythrophagocytic function of splenic macrophages.

Reduced erythrophagocytosis leads to RBCs retention in the spleen under HH exposure

Based on the reduced RPMs and erythrophagocytosis caused by HH exposure in spleen, we next investigated whether RBCs were retained in spleen after HH exposure. Initial examination involved detecting RBCs in the spleen post HH exposure, both with and without perfusion. HE staining (Figure 6, A-B) and Band 3 immunostaining in situ (Figure 6, C-D, G-H) revealed a significant increase in RBCs numbers in the spleen following 7 and 14 days of HH exposure. Furthermore, we quantified RBCs retention by employing Wright-Giemsa composite staining on single splenic cells post-perfusion at both 7- and 14-days post HH exposure. The results consistently indicated a substantial elevation in RBC counts within the spleen (Figure 6, E-F). To enhance the specificity of our investigation, we labelled RBCs *in vitro* with PKH67 and then administered them to mice. Following HH exposure for 7 and 14 days,

483 spleen sections were analyzed without perfusion to detect retained PKH67-labeled
484 RBCs. Fluorescence detection techniques was utilized, revealing a marked increase in
485 PKH67-labeled RBCs post HH exposure (Figure 6, I-J). These results collectively
486 confirm a pronounced impairment in erythrophagocytosis within the spleen under HH
487 conditions. This is evidenced by the observed increase in RBCs deformation and
488 retention following 7 and 14 days of HH exposure. The data thus suggest that HH
489 exposure leads to an increase in RBCs retention in the spleen, highlighting significant
490 alterations in splenic function and RBCs dynamics under hypoxic conditions.
491
492 **HH induced reduction in erythrophagocytosis leads to a decrease in the capacity**
493 **of iron processing in the spleen**
494 To investigate the hypothesis that increased retention of RBCs in the spleen due to
495 HH exposure is a result of impaired erythrophagocytosis by RPMs, we employed a
496 series of experiments. Initially, RBCs were labelled with PKH67 cell linker and then
497 injected into mice. Subsequently, Tuftsin was administered to stimulate the phagocytic
498 activity of macrophages. After 1 h, 1 day, 3 days, 5 days, or 7 days of NN exposure,
499 PKH67 fluorescence was analyzed via flow cytometry. The findings demonstrated a
500 gradual reduction in PKH67 fluorescence over the course of NN exposure; however, a
501 significant decrease in PKH67 fluorescence was noted in the spleen following Tuftsin
502 administration compared to the NN group. This observation suggested that RBC
503 lifespan is diminished following enhanced erythrophagocytosis (as presented in
504 Figure 7, A-B). Further investigation was conducted on the ability of the spleen to

regulate heme iron recycling under HH conditions through immunofluorescence and iron staining (Figure 7C). The results, as illustrated in Figure 7D, indicated that both F4/80 expression and iron deposition in the red pulp of the spleen were notably reduced following HH exposure, compared to the NN group. Contrastingly, Tuftsin administration under HH conditions resulted in an upsurge in F4/80 expression and iron deposition in the red pulp (Figure 7, E-F). These findings collectively suggest that the splenic capacity for erythrocyte phagocytosis and subsequent heme iron recycling is significantly compromised under HH conditions, primarily due to a reduction in RPMs. This reduced erythrophagocytic capacity of the spleen under HH exposure is a critical factor contributing to the decreased efficiency of iron processing and increased RBCs retention in this organ.

HH exposure induces iron mobilization and ferroptosis in the spleen

To elucidate the precise mechanisms underlying the macrophage reduction caused by HH, we examined the expression of proteins related to iron metabolism and ferroptosis in mice treated with HH and analyzed the corresponding gene expression in peripheral blood mononuclear cells (PBMCs) from healthy humans acutely exposed to HA conditions using GEO data (No. GSE46480). The results showed that, compared to the NN group, the expression levels of HO-1, Ft-L, Ft-H, NCOA4, and xCT were decreased, while Fpn, TfR, and ACSL4 expressions were significantly increased after 7 and 14 days of HH exposure (Figure 8, A-B, D-E; Figure S3, A-D). Apart from NCOA4, the alterations in gene expressions related to iron metabolism

and ferroptosis in PBMCs were consistent with our Western blot results (Figure 8, C and F). The GPX4 gene and protein expressions remained largely unchanged in both human PBMCs and mouse spleens. The changes in iron metabolism- and ferroptosis-related genes in PBMCs reflect the protein changes in the spleen under HH exposure. We detected Fe^{2+} and lipid ROS levels in the spleen by flow cytometry, and quantified MDA, GSH, and Cys levels using biochemical detection kits. As depicted in Figure 8, G and H; Figure S3, I-K, the Fe^{2+} (Figure 8G; Figure S3, E and F) and lipid ROS (Figure 8H; Figure S3, G and H) levels in the spleen increased significantly after HH exposure. Additionally, the MDA content (Figure 8I; Figure S3I) in the spleen increased, whereas Cys (Figure 8J; Figure S3J) and GSH (Figure 8K; Figure S3K) levels significantly decreased after HH exposure. To ascertain the increased Fe^{2+} primarily emanated from the red pulp, we detected Fe^{2+} deposition and distribution in the spleen by Lillie stain following 7 and 14 days of HH exposure (Figure 8, L-M; Figure S3, L-M). These results demonstrated increased Fe^{2+} primarily deposited in the red pulp of the spleen. Taken together, these findings suggest that iron mobilization in the spleen was enhanced and ferroptosis was induced after 7 days of HH exposure.

Hypoxia induces ferroptosis in primary splenic macrophages

To investigate whether hypoxia exposure can trigger ferroptosis in macrophages, we measured alterations in Fe^{2+} and lipid ROS levels, cell viability, phagocytosis, and ferroptosis-related protein expressions in primary splenic macrophages under hypoxia

in the presence of a ferroptosis inhibitor (Fer-1). As depicted in Figure 9, compared with the normoxia control group (Nor), Fe^{2+} (Figure 9, A-C) and lipid ROS (Figure 9, D-E) levels significantly increased, whereas the number of viable cells (Figure 9, G-H) and phagocytosis ability (Figure 9I) significantly decreased after 24 h of hypoxia (Hyp) treatment. In addition, prolonged hypoxia exposure led to a gradual increase in ACSL4 expression, while xCT and GPX4 expressions decreased (Figure 9F). Fer-1 mitigated the increase in Fe^{2+} content (Figure 9, J-K) and reversed the expression changes in ACSL4, xCT, and GPX4 induced by hypoxia exposure (Figure 9, L-O). Simultaneously, Fer-1 reversed the alterations in MDA, Cys, and GSH levels induced by hypoxia (Figure 9, P-R). These findings confirm that hypoxia induced ferroptosis in primary splenic macrophages.

Discussion

The purpose of this study was to explore the effects and mechanisms of HA/HH exposure on erythrophagocytosis and iron circulation in mouse spleens. Here, we used an HH chamber to simulate 6000 m HA exposure and found that HH exposure induced iron mobilization and activated ferroptosis in the spleen, especially in RPMs, which subsequently inhibited the phagocytosis and clearance of RBCs. Finally, chronic exposure to HA/HH may promote the retention of RBCs in the spleen, cause splenomegaly, advance RBC production, and promote the occurrence and development of HAPC.

RBCs/erythrocytes are the carriers of oxygen and the most abundant cell type in the

body. Erythrocytes are rapidly increased by triggering splenic contraction in acute HA/HH exposure [23] and stimulating erythropoiesis in subsequent continuous or chronic HA/HH exposure. Changes in spleen morphology and size are closely related to the spleen's ability to recover RBCs [24], and studies have shown that the spleen is in a contraction state after short-term exposure to HA/HH, and approximately 40% of the increase in RBCs is due to the contraction of the spleen [23, 25, 26]. In the present study, mice were treated under HH to mimic HA exposure (mainly mimicking the low oxygen partial pressure environment of 6000 m HA) for different times according to other studies [27, 28]. Our results showed that HH exposure significantly increased the number of RBCs and HGB contents. However, short-term (1 day) HH exposure caused spleen contraction and induced splenomegaly after 3 days of HH treatment. This contraction can trigger an immediate release of RBCs into the bloodstream in instances of substantial blood loss or significant reduction of RBCs. Moreover, elevated oxygen consumption rates in certain animal species can be partially attributed to splenic contractions, which augment haematocrit levels and the overall volume of circulating blood, thereby enhancing venous return and oxygen delivery [29, 30]. Thus, we hypothesized that the body, under such conditions, is incapable of generating sufficient RBCs promptly enough to facilitate enhanced oxygen delivery. Consequently, the spleen reacts by releasing its stored RBCs through splenic constriction, leading to a measurable reduction in spleen size. These results are consistent with other research results; that is, HH or HA exposure affects spleen morphology and further affects RBCs counts and HGB levels [31-33].

HAPC is a common chronic HA disease characterized by excessive proliferation of RBCs caused by HH conditions [34]. Under physiological conditions, RBC homeostasis is maintained by balancing erythropoiesis and erythrocyte clearance [4]. The ability of RBC disposal in the spleen for iron recycling under HA/HH exposure was important to RBC regeneration in BM [35]. Thus, we hypothesized that erythrophagocytosis and iron recycling in the spleen were altered by HA/HH exposure and further disturbed RBC homeostasis and affected the progression of HAPC. We found that compared with sham group mice, HH significantly increased the contents of RBCs and HGB in the blood of splenectomy mice. This strongly verified that the spleen is a key organism that maintains RBC magnitude within a certain range of physiological statuses under HA/HH conditions.

As originally proposed by Metchnikoff in the 19th century, macrophages, especially RPMs, play a pivotal role in the regulation of RBCs and iron homeostasis [36, 37]. We detected the macrophage population in the spleen and found that HH exposure for 7 and 14 days reduced the total macrophages in the spleen. We next observed whether the migration and differentiation of monocytes from the BM to the spleen supplemented the reduced macrophages after HH treatment and maintained their homeostasis. It is well known that splenic erythrophagocytosis is a dynamic process [4]. Upon phagocytosing erythrocytes in macrophages, spleen tissue (including macrophages and fibroblasts) produces the chemokine C–C motif chemokine ligand 2 and 7 (CCL2 and CCL7) to recruit blood monocytes to the spleen [38, 39]. In our study, the expression of CCL2, CCL7, and Csf1 in the spleen

decreased after 7 and 14 days of HH exposure. Furthermore, we found that HH exposure inhibited Ly6C^{hi} monocyte migration from the BM to spleen, where these cells subsequently differentiated into RPMs. The combination of decreased splenic RPMs, along with the reduced BM-derived Ly6C^{hi} monocytes, suggests that the homeostasis of the RPMs population in circulating monocytes was also inhibited after the depletion of RPMs induced by HH exposure. The observed decrease in monocytes within the BM is likely attributable to the fact that monocytes and precursor cells for RBCs both originate from the same hematopoietic stem cells within the BM [40]. As such, the differentiation to monocyte is reduced under hypoxic conditions, which may subsequently cause a decrease in migration to spleen.

HO-1 is a pivotal antioxidant and cytoprotective enzyme, instrumental in catalyzing the degradation of heme, thereby maintaining heme homeostasis and mitigating free heme-induced toxicity [41]. Notably, it has been posited that mice deficient in HO-1 exhibit a significant depletion of RPMs, emphasizing the important role of this enzyme in the development and maintenance of RPM after RBCs clearance [42]. In our study, the observed decrease in HO-1 protein levels in the red pulp suggests a potential reduction in the number of macrophages induced by HH exposure. This inference is made despite the general understanding that HO-1 expression is typically upregulated by hypoxia-inducible factor 1 (HIF-1) under hypoxic conditions [43, 44]. Along with the decrease in the number of macrophages caused by HH, we also noticed that the phagocytic ability of macrophages in the spleen is inhibited, as evidenced both *in vitro* and *in vivo*. Furthermore, the administration of tufftsin

markedly enhanced heme iron processing in the spleen under HH conditions. However, our findings appear to diverge from those reported by Anand et al., which suggested an increase in macrophage phagocytosis under hypoxic conditions, mediated by HIF-1α [45]. This discrepancy may stem from the differing methodologies employed; whereas Anand et al. utilized intermittent hypoxia in their research, our study was characterized by consistent hypoxia. However, it should be acknowledged that using HO-1 expression as an alternative marker to quantify macrophage numbers is not without limitations. Variations in HO-1 expression per cell can yield misleading results, and the localization of this effect to the red pulp does not definitively equate to a conclusion applicable to macrophages, given the inherent heterogeneity of this region and the spleen overall. Considering the multifaceted nature of spleen function and cellular dynamics under hypoxic stress, this complexity requires careful interpretation of our data.

Macrophages play a crucial role in maintaining erythrocyte homeostasis, partially due to their function in digesting the HGB content of cleared RBCs and recycling the iron back to erythroid progenitors for heme synthesis and HGB production [46]. In mammals, most of the bodily iron exists in the form of heme, with the most substantial pool comprising HGB [47]. HGB contains four prosthetic hemoglobins, and each mature RBC is thought to contain approximately 1.2×10^9 heme moieties [46]. As previously mentioned, most of the iron required to sustain erythropoiesis is derived from recycled RBCs. In general, RPMs are equipped with molecular machinery capable of neutralizing the toxic effects of heme and metabolizing iron [48,

49]. Nonetheless, any disruptions in the process of erythrophagocytosis, the uptake and degradation of erythrocytes by macrophages, could potentially result in abnormal iron metabolism, potentially manifesting as conditions such as anemia or iron overload [48]. The release of heme upon processed RBCs constitutes a permanent and considerable threat for iron cytotoxicity in macrophages and may eventually result in a specific form of programmed cell death termed ferroptosis [50], which may cause decreased cell counts [51, 52].

Accordingly, we investigated the iron metabolism status and explored ferroptosis in spleen/macrophages after HH/hypoxia treatment and found that HH exposure prompted iron mobilization, especially in ferritinophagy and lipid peroxidation in the spleen. Interestingly, we found that all gene expression changes in PBMCs after acute HA exposure in humans, except for NCOA4, were similar to those in the spleen of mice exposed to HH for 7 and 14 days. This is probably because NCOA4 in the spleen mediates iron release from Ft-L and facilitates iron reuse, while PBMCs do not possess this function *in vivo*. These results not only indicated that HH exposure induces spleen ferroptosis but also implied that the gene expression changes in PBMCs under HA/HH may reflect RBC processing functions in the spleen and further indicate the iron metabolism status in the clinic. We further found that the exact mechanism of macrophage ferroptosis induced by HH exposure was caused by increased Fe^{2+} and decreased antioxidative system expression, which finally resulted in lipid peroxidation of macrophages. It has been proposed that heme catabolism by HO-1 protects macrophages from oxidative stress [48]. The enhanced ROS and lipid

peroxidation *in vivo* were also consistent with the decreased HO-1 expression in the spleen. In addition, 1% hypoxia treatment induced ferroptosis *in vitro*, which was reduced by treatment with ferrostatin-1, a ferroptosis inhibitor. However, our data were inconsistent with the study of Fuhrmann *et al*., which reported that hypoxia inhibits ferritinophagy and protects against ferroptosis [53]. We hypothesized that the enhanced iron demand for new RBCs regeneration in BM caused by HH leads to a decrease in the expression of NCOA4 and Ft-L proteins in the spleen. On the other hand, hypoxia inhibited anti-ferroptosis system expression, including reduced Gpx4 expression and increased lipid ROS production. The results were supported by the group of Youssef LA *et al*, who reported that increased erythrophagocytosis induces ferroptosis in RPMs in a mouse model of transfusion [54]. However, as most studies have reported, ferroptosis is not only characterized by increased lipid ROS but also significantly shrinking mitochondria [55]. We never found shrinking mitochondria in RPMs after HH exposure (data not shown). Gao *et al*. proposed that mitochondria played a crucial role in cysteine deprivation-induced ferroptosis but not in that induced by inhibiting glutathione peroxidase-4 (GPX4), the most downstream component of the ferroptosis pathway [56]. Interestingly, in our *in vivo* study, Gpx4 expression was also not changed after HH exposure. It is still not clear whether mitochondria are involved in ferroptosis. Whether HH treatment caused mitochondrial swelling directly and the exact mechanism involved in this process still need to be further investigated.

It is also possible that the spleen may adapt to the increased load of RBCs by

expanding the red pulp, leading to splenomegaly [57]. The red pulp is highly vascular and contains numerous sinuses lined with macrophages [58]. This expansion could potentially accommodate a greater number of RBCs, thus enhancing the splenic capacity for erythrophagocytosis and iron recycling. However, these compensatory mechanisms may be insufficient or become overwhelmed over time, leading to pathological conditions such as HAPC. Further research is necessary to fully understand the consequences of splenic ferroptosis on RBC homeostasis and how these effects could be mitigated or reversed. Finally, as these observations are based on experimental models, they should be corroborated in human studies to assess their clinical relevance and potential implications for managing conditions related to high altitude exposure. The potential for therapeutic interventions that target ferroptosis, erythrophagocytosis, and iron recycling should also be explored, as these could provide new avenues for treating HAPC and other conditions related to HA exposure.

Based on the above experiments, we propose the "spleen theory" of HAPC as depicted in Figure 10. It hypothesizes that HH exposure precipitates ferroptosis within the spleen, particularly affecting RPMs. This process, in turn, impedes erythrophagocytosis, RBCs clearance, HGB processing, and iron recycling. Consequently, this leads to an accumulation of RBCs within the spleen, exacerbating splenomegaly and perpetuating the production of RBCs under HH conditions. The "spleen theory" of HAPC provides a novel perspective on the physiological responses to hypoxia and highlights the role of the spleen as a vital organ in managing erythrocyte homeostasis under high altitude/hypoxic conditions. These findings may

be clinically relevant to the pathological conditions of HAPC progression.

Abbreviations

BM: bone marrow; Cys: Cysteine; GSH: Glutathione; Ft-L: Ferritin light chains; Fpn: Ferroportin; Ft: Ferritin; HH: Hypobaric hypoxia; HA: High-altitude; HAPC: High-altitude polycythemia; HO-1: Heme oxygenase-1; HCT: Haematocrit; HGB: Haemoglobin; HIF-1a: Hypoxia inducible factor 1 a; MCH: Mean corpuscular haemoglobin; MDA: Malondialdehyde; NN: Normobaric normoxia; NCOA4: nuclear receptor coactivator 4; PBMCs: peripheral blood mononuclear cells; RBC: Red blood cell; RPM: Red pulp macrophage; TfR1: Transferrin receptor 1; Tf: Transferrin; TfR: Transferrin receptor.

Author contributions

QQL and GHW conceived, organized, and designed the study. YQG supervised the work. WPY, MQL, JD and JYL performed the experiments. WPY, GW and BL contributed to the analysis of data. QQL and GHW prepared, wrote, and revised the manuscript. All authors contributed to read, and approved the submitted version.

Funding

This work was supported by Natural Science Foundation of China (Grants 32271228, 81873924 and 82171190), Open Cooperation Program from Key Laboratory of Extreme Environmental Medicine, Ministry of Education (KL2019GY011), China Postdoctoral Science Foundation (2020M673649), Cultivate Candidate of the Jiangsu Province “333” Project.

Availability of data and materials

The datasets used and/or analysed during the current study are available from the corresponding author on reasonable request.

Declarations

Ethics approval and consent to participate

All animal care and experimental protocols were carried out according to the Chinese Animal Management Rules of the Ministry of Health and were authorized by the Animal Ethics Committees of Nantong University research program protocol #S20190219-011. The results of the study are presented clearly, honestly, and without fabrication, falsification, or inappropriate data manipulation.

Consent for publication

Not applicable.

Competing interests

The authors have no relevant financial or non-financial interests to disclose.

Author details

[1]Department of Physiology and Hypoxic Biomedicine, Institute of Special Environmental Medicine and Co-innovation Center of Neuroregeneration, Nantong University, 9 Seyuan Road, Chongchuan District, Nantong, Jiangsu 226019, China. [2]College of High-Altitude Military Medicine, Institute of Medicine and Hygienic Equipment for High Altitude Region, Army Medical University, Chongqing 400038, China. [3]Key Laboratory of Extreme Environmental Medicine and High-Altitude Medicine, Ministry of Education of China, Chongqing 400038, China. [4]Department of Neurosurgery, Southwest Hospital, Army Medical University, Chongqing, Chongqing 400038, China.

References

1. Pérez-Padilla R. Impact of moderate altitude on lung diseases and risk of high altitude illnesses. Revista de investigacion clinica; organo del Hospital de Enfermedades de la Nutricion. 2022;74(5):232-43.
2. Liu X, Zhang H, Yan J, Li X, Li J, Hu J, et al. Deciphering the Efficacy and Mechanism of Astragalus membranaceus on High Altitude Polycythemia by Integrating Network Pharmacology and In Vivo Experiments. Nutrients. 2022;14(23).
3. Tymko MM, Lawley JS, Ainslie PN, Hansen AB, Hofstaetter F, Rainer S, et al. Global Reach 2018 Heightened α-Adrenergic Signaling Impairs Endothelial Function During Chronic Exposure to Hypobaric Hypoxia. Circulation research. 2020;127(2):e1-e13.
4. Dzierzak E, Philipsen S. Erythropoiesis: development and differentiation. Cold Spring Harb Perspect Med. 2013;3(4):a011601.
5. Robach P, Hansen J, Pichon A, Meinild Lundby AK, Dandanell S, Slettaløkken Falch G, et al. Hypobaric live high-train low does not improve aerobic performance more than live low-train low in cross-country skiers. Scandinavian journal of medicine & science in sports. 2018;28(6):1636-52.
6. Yang W, Li J, Hu J, Yuan X, Ding J, Jiang H, et al. Hypobaric hypoxia induces iron mobilization from liver and spleen and increases serum iron via activation of ghrelin/GHSR1a/MAPK signalling pathway in mice. Scientific reports. 2023;13(1):20254.
7. Slusarczyk P, Mleczko-Sanecka K. The Multiple Facets of Iron Recycling. Genes. 2021;12(9).
8. Qiang Y, Sissoko A, Liu ZL, Dong T, Zheng F, Kong F, et al. Microfluidic study of retention and elimination of abnormal red blood cells by human spleen with implications for sickle cell disease. Proc Natl Acad Sci U S A. 2023;120(6):e2217607120.
9. Wirth F, Lubosch A, Hamelmann S, Nakchbandi IA. Fibronectin and Its Receptors in Hematopoiesis. Cells. 2020;9(12).
10. Slusarczyk P, Mandal PK, Zurawska G, Niklewicz M, Chouhan K, Mahadeva R, et al. Impaired iron recycling from erythrocytes is an early hallmark of aging. eLife. 2023;12.
11. Vahedi A, Bigdelou P, Farnoud AM. Quantitative analysis of red blood cell membrane phospholipids and modulation of cell-macrophage interactions using cyclodextrins. Scientific reports. 2020;10(1):15111.
12. Nemeth E, Ganz T. Hepcidin-Ferroportin Interaction Controls Systemic Iron Homeostasis. Int J Mol Sci. 2021;22(12).
13. Hidalgo D, Bejder J, Pop R, Gellatly K, Hwang Y, Maxwell Scalf S, et al. EpoR stimulates rapid cycling and larger red cells during mouse and human erythropoiesis. Nat Commun. 2021;12(1):7334.
14. Wang W, Grier DD, Woo J, Ward M, Sui G, Torti SV, et al. Ferritin H is a novel marker of early erythroid precursors and macrophages. Histopathology.

2013;62(6):931-40.
15. Finazzi D, Arosio P. Biology of ferritin in mammals: an update on iron storage, oxidative damage and neurodegeneration. Archives of toxicology. 2014;88(10):1787-802.
16. Bellelli R, Federico G, Matte' A, Colecchia D, Iolascon A, Chiariello M, et al. NCOA4 Deficiency Impairs Systemic Iron Homeostasis. Cell Reports. 2016;14(3):411-21.
17. von Krusenstiern AN, Robson RN, Qian N, Qiu B, Hu F, Reznik E, et al. Identification of essential sites of lipid peroxidation in ferroptosis. Nature chemical biology. 2023.
18. Corazza GR, Zoli G, Di Sabatino A, Ciccocioppo R, Gasbarrini G. A reassessment of splenic hypofunction in celiac disease. The American journal of gastroenterology. 1999;94(2):391-7.
19. Liu Z, Lv X, Yang B, Qin Q, Song E, Song Y. Tetrachlorobenzoquinone exposure triggers ferroptosis contributing to its neurotoxicity. Chemosphere. 2021;264(Pt 1):128413.
20. Jiang H, Zhang X, Yang W, Li M, Wang G, Luo Q. Ferrostatin-1 Ameliorates Liver Dysfunction via Reducing Iron in Thioacetamide-induced Acute Liver Injury in Mice. Frontiers in pharmacology. 2022;13:869794.
21. Luo Q, Hu J, Yang G, Yuan X, Chen Z, Wang D, et al. Fasting Increases Iron Export by Modulating Ferroportin 1 Expression Through the Ghrelin/GHSR1alpha/MAPK Pathway in the Liver. Biol Trace Elem Res. 2021;199(1):267-77.
22. Nébor D, Graber JH, Ciciotte SL, Robledo RF, Papoin J, Hartman E, et al. Mutant KLF1 in Adult Anemic Nan Mice Leads to Profound Transcriptome Changes and Disordered Erythropoiesis. Scientific reports. 2018;8(1):12793.
23. Schagatay E, Lunde A, Nilsson S, Palm O, Lodin-Sundstrom A. Spleen contraction elevates hemoglobin concentration at high altitude during rest and exercise. Eur J Appl Physiol. 2020;120(12):2693-704.
24. Khairullah S, Jackson N. Markers of ineffective erythropoiesis in non-transfusion dependent β-thalassaemia. Med J Malaysia. 2021;76(1):41-5.
25. Alafi MH, Cook SF. Role of the spleen in acclimatization to hypoxia. Am J Physiol. 1956;186(2):369-72.
26. Richardson M, Lodin A, Reimers J, Schagatay E. Short-term effects of normobaric hypoxia on the human spleen. European journal of applied physiology. 2008;104(2):395-9.
27. Lin HJ, Wang CT, Niu KC, Gao C, Li Z, Lin MT, et al. Hypobaric hypoxia preconditioning attenuates acute lung injury during high-altitude exposure in rats via up-regulating heat-shock protein 70. Clin Sci (Lond). 2011;121(5):223-31.
28. Brent MB, Emmanuel T, Simonsen U, Bruel A, Thomsen JS. Hypobaric hypoxia deteriorates bone mass and strength in mice. Bone. 2022;154:116203.
29. Dane DM, Hsia CC, Wu EY, Hogg RT, Hogg DC, Estrera AS, et al. Splenectomy impairs diffusive oxygen transport in the lung of dogs. Journal of

applied physiology (Bethesda, Md : 1985). 2006;101(1):289-97.
30. Longhurst JC, Musch TI, Ordway GA. O2 consumption during exercise in dogs--roles of splenic contraction and alpha-adrenergic vasoconstriction. Am J Physiol. 1986;251(3 Pt 2):H502-9.
31. Holmstrom PK, Bird JD, Thrall SF, Kalker A, Herrington BA, Soriano JE, et al. The effects of high altitude ascent on splenic contraction and the diving response during voluntary apnoea. Exp Physiol. 2021;106(1):160-74.
32. Holmstrom P, Mulder E, Starfelt V, Lodin-Sundstrom A, Schagatay E. Spleen Size and Function in Sherpa Living High, Sherpa Living Low and Nepalese Lowlanders. Front Physiol. 2020;11:647.
33. Pernett F, Schagatay F, Vildevi C, Schagatay E. Spleen Contraction During Sudden Eupneic Hypoxia Elevates Hemoglobin Concentration. Front Physiol. 2021;12:729123.
34. Wang Z, Tenzing N, Xu Q, Liu H, Ye Y, Wen Y, et al. Apoptosis is one cause of thrombocytopenia in patients with high-altitude polycythemia. Platelets. 2023;34(1):2157381.
35. Pivkin IV, Peng Z, Karniadakis GE, Buffet PA, Dao M, Suresh S. Biomechanics of red blood cells in human spleen and consequences for physiology and disease. Proc Natl Acad Sci U S A. 2016;113(28):7804-9.
36. Wynn TA, Chawla A, Pollard JW. Macrophage biology in development, homeostasis and disease. Nature. 2013;496(7446):445-55.
37. Gammella E, Buratti P, Cairo G, Recalcati S. Macrophages: central regulators of iron balance. Metallomics. 2014;6(8):1336-45.
38. Zhang L, Patel S, Soulakova JN, Caldwell CC, St Pierre Schneider B. Mild hypobaric hypoxia influences splenic proliferation during the later phase of stress erythropoiesis. Exp Biol Med (Maywood). 2022;247(6):509-18.
39. Bellomo A, Mondor I, Spinelli L, Lagueyrie M, Stewart BJ, Brouilly N, et al. Reticular Fibroblasts Expressing the Transcription Factor WT1 Define a Stromal Niche that Maintains and Replenishes Splenic Red Pulp Macrophages. Immunity. 2020;53(1):127-42 e7.
40. Bapat A, Schippel N, Shi X, Jasbi P, Gu H, Kala M, et al. Hypoxia promotes erythroid differentiation through the development of progenitors and proerythroblasts. Experimental hematology. 2021;97:32-46.e35.
41. Vijayan V, Wagener F, Immenschuh S. The macrophage heme-heme oxygenase-1 system and its role in inflammation. Biochem Pharmacol. 2018;153:159-67.
42. Kovtunovych G, Eckhaus MA, Ghosh MC, Ollivierre-Wilson H, Rouault TA. Dysfunction of the heme recycling system in heme oxygenase 1-deficient mice: effects on macrophage viability and tissue iron distribution. Blood. 2010;116(26):6054-62.
43. Lee PJ, Jiang BH, Chin BY, Iyer NV, Alam J, Semenza GL, et al. Hypoxia-inducible factor-1 mediates transcriptional activation of the heme oxygenase-1 gene in response to hypoxia. J Biol Chem. 1997;272(9):5375-81.
44. Dawn B, Bolli R. HO-1 induction by HIF-1: a new mechanism for delayed

cardioprotection? Am J Physiol Heart Circ Physiol. 2005;289(2):H522-4.
45. Anand RJ, Gribar SC, Li J, Kohler JW, Branca MF, Dubowski T, et al. Hypoxia causes an increase in phagocytosis by macrophages in a HIF-1alpha-dependent manner. J Leukoc Biol. 2007;82(5):1257-65.
46. Korolnek T, Hamza I. Macrophages and iron trafficking at the birth and death of red cells. Blood. 2015;125(19):2893-7.
47. Hamza I, Dailey HA. One ring to rule them all: Trafficking of heme and heme synthesis intermediates in the metazoans. Bba-Mol Cell Res. 2012;1823(9):1617-32.
48. Soares MP, Hamza I. Macrophages and Iron Metabolism. Immunity. 2016;44(3):492-504.
49. Ganz T. Macrophages and Iron Metabolism. Microbiol Spectr. 2016;4(5).
50. Dixon SJ, Lemberg KM, Lamprecht MR, Skouta R, Zaitsev EM, Gleason CE, et al. Ferroptosis: An Iron-Dependent Form of Nonapoptotic Cell Death. Cell. 2012;149(5):1060-72.
51. Zhang P, Chen L, Zhao QQ, Du XX, Bi MX, Li Y, et al. Ferroptosis was more initial in cell death caused by iron overload and its underlying mechanism in Parkinson's disease. Free Radical Bio Med. 2020;152:227-34.
52. Chen X, Yu CH, Kang R, Tang DL. Iron Metabolism in Ferroptosis. Front Cell Dev Biol. 2020;8.
53. Fuhrmann DC, Mondorf A, Beifuss J, Jung M, Brune B. Hypoxia inhibits ferritinophagy, increases mitochondrial ferritin, and protects from ferroptosis. Redox Biol. 2020;36:101670.
54. Youssef LA, Rebbaa A, Pampou S, Weisberg SP, Stockwell BR, Hod EA, et al. Increased erythrophagocytosis induces ferroptosis in red pulp macrophages in a mouse model of transfusion. Blood. 2018;131(23):2581-93.
55. Xie Y, Hou W, Song X, Yu Y, Huang J, Sun X, et al. Ferroptosis: process and function. Cell Death Differ. 2016;23(3):369-79.
56. Gao M, Yi J, Zhu J, Minikes AM, Monian P, Thompson CB, et al. Role of Mitochondria in Ferroptosis. Mol Cell. 2019;73(2):354-63 e3.
57. Li H, Lu L, Li X, Buffet PA, Dao M, Karniadakis GE, et al. Mechanics of diseased red blood cells in human spleen and consequences for hereditary blood disorders. Proc Natl Acad Sci U S A. 2018;115(38):9574-9.
58. Mebius RE, Kraal G. Structure and function of the spleen. Nature Reviews Immunology. 2005;5(8):606-16.

Figure legends

Figure 1. HH exposure promotes the induction of erythrocytosis in mice. C57BL/6 mice were subjected to either normobaric normoxia (NN) or hypobaric hypoxia (HH) conditions for durations of 3, 7, and 14 days. After these treatments, blood samples were collected for a comprehensive analysis. (**A**) Morphological evaluation of RBCs was conducted via blood smear examination (Wright staining). Routine hematological assessments were performed, encompassing RBCs counts (**B**), hemoglobin (HGB) levels (**C**), hematocrit (HCT) percentages (**D**), and mean corpuscular hemoglobin (MCH) content (**E**). (**F**) Flow cytometric analysis was employed to identify TO-positive cells, indicative of reticulocytes, in the whole blood samples. (**G**) The proportions of TO-positive RBCs in the blood were depicted in bar graphs. The data are presented as means ± SEM for each group (n = 5 per group). Statistical significance is denoted by * $P < 0.05$, ** $P < 0.01$, *** $P < 0.001$, relative to the NN group or as specified.

Figure 2. The spleen plays an important role in suppressing the immoderate increase in RBCs under HH conditions. C57BL/6 mice with or without splenectomy were treated with NN and HH for varying durations, and the spleen and blood were collected for subsequent analyses. (**A**) Morphological observation, (**B**) Spleen volume, and (**C**) spleen weight was determined. (**D-H**) Blood observation and hematological index detection followed. Data are expressed as the means ± SEM (n = 9 per group); * $P < 0.05$, ** $P < 0.01$, *** $P < 0.001$ versus the NN group or the

indicated group.

Figure 3. HH exposure results in a decrease in the number of splenic macrophages. C57BL/6 mice were treated with NN and HH for 7 or 14 days, and the spleen and blood were collected for subsequent analysis. (**A**) Calcein/PI double staining was analysed by flow cytometry to assess cell viability. (**B and C**) The bar graphs represent the proportions of cell death in total splenic cell population. (**D**) Uniform Manifold Approximation and Projection (UMAP) provided a visualization of spleen cell clusters, with each color representing a unique cluster characterized by specific gene expression profiles. (**E**) Comparative analysis of the proportions of distinct macrophage clusters in spleens from NN- and HH-treated mice. (**F**) Presentation of individual macrophages from spleens of mice treated with either NN or HH. (**G**) Analysis of F4/80 and CD11b expression in splenic cells, conducted via flow cytometry. (**H**) qPCR analysis evaluated CCL2 and CCL7 gene expression in the spleen. (**I**) qPCR analysis of Csf1 and Csf2 expression levels in the spleen. (**J**) Flow cytometry facilitated the detection of CD11b and Ly6C double-stained cells in BM and spleen. (**K-L**) Bar graphs represent the proportions of $CD11b^{hi}Ly6C^{hi}$ cells in the BM, while (**M-N**) delineate those in the spleen. (**O**) HO-1 and F4/80 expression levels in the spleen were monitored after 0 (NN), 7, and 14 days of HH exposure. (**P**) The relative fluorescence intensities of HO-1 and (**Q**) F4/80, as outlined in (**O**), were quantitatively assessed. Data are expressed as means ±SEM for each group (n = 3 per group). Statistical significance is indicated by * $P < 0.05$, ** $P < 0.01$, *** $P < 0.001$

when compared to the NN group or the indicated group.

Figure 4. HH exposure decreases RBCs clearance both in the blood and spleen. (**A and B**) Flow cytometry measurements illustrated the proportions of FITC-stained RBCs in blood and spleen, respectively, after 7 and 14 days of HH exposure. (**C and D**) Bar graphs depicted the quantified proportions of FITC-positive RBCs in both blood and spleen, respectively. Further, (**E and F**) presented flow cytometry assessments of the proportions of PKH67-labelled RBCs in blood and spleen following 7 and 14 days of HH exposure. The corresponding proportions of PKH67-positive RBCs in blood (**G**) and spleen (**H**) were also shown in bar graph format. The data are expressed as means ±SEM for each experimental group (n = 3 per group). Statistical significance is denoted with * $P < 0.05$, ** $P < 0.01$, *** $P < 0.001$, relative to the NN group or as specified in the graph legends. This compilation of data underlines the impact of HH exposure on the reduction of RBCs clearance in both blood and splenic compartments.

Figure 5. HH exposure reduces erythrophagocytosis in the spleen. Mice were administered PKH67-labeled RBCs, followed by exposure to HH for durations of 7 and 14 days. (**A**) Flow cytometry was employed to analyze the proportions of RPMs (identified as F4/80^{+}CD11b^{-}) and PKH67-positive RPMs in the spleen post-exposure. (**B** and **C**) Bar graphs represent the quantified proportions of RPMs (F4/80^{+}CD11b^{-}) and PKH67-positive RPMs in the spleen, respectively. (**D**) The spleens were subjected

to immunofluorescence analysis to detect F4/80 in conjunction with PKH67 fluorescence post-perfusion at 7 and 14 days following HH exposure. (**E**) Subsequent quantification of the number of PKH67-positive F4/80^{hi} cells in the spleen, as depicted in (**D**), was conducted. The data derived from these analyses are expressed as means ±SEM for each group (n = 3 per group). Statistical significance is denoted with * $P < 0.05$, and *** $P < 0.001$, relative to the indicated group in the graph legends.

Figure 6. HH exposure increases RBCs retention in the spleen. (**A**) HE staining was utilized to examine the presence of RBCs in the spleen post-perfusion at 7 and 14 days following HH exposure. (**B**) The number of RBCs present in the spleen, as observed in (**A**), was quantitatively assessed. (**C** and **G**) Immunohistochemical and immunofluorescent analyses using Band 3 staining were conducted to evaluate RBCs content in the spleen post-perfusion at 7 and 14 days of HH exposure. (**D** and **H**) The expression levels of Band 3 in the spleen, as shown in (**C and G**), were quantified. (**E**) Wright-Giemsa composite staining was performed on splenic cells following HH exposure for durations of 0 (NN), 7, and 14 days. (**F**) The proportion of RBCs within the perfused splenic cell population was determined. (**I**) Detection of PKH67 fluorescence in the spleen, without perfusion, was conducted after administering PKH67-labeled RBCs and subjecting them to HH exposure for 7 and 14 days. (**J**) The number of PKH67-positive RBCs within the spleen, as outlined in (**I**), was quantified. Data presented in this figure are expressed as means ±SEM for each experimental group (n = 3 per group). Statistical significance is indicated by * $P < 0.05$, ** $P <$

0.01, *** $P < 0.001$ when compared to the NN group or as specified.

Figure 7. Impaired erythrophagocytosis of RBCs after HH exposure leads to a decrease in iron processing capacity in the spleen. To stimulate phagocytosis of macrophages, Tuftsin was administered immediately following the injection of PKH67-labeled RBCs into mice. Subsequent to various exposure durations under NN conditions (1 h, 1, 3, 5, or 7 days), (**A**) PKH67 fluorescence within the spleen was measured using flow cytometry. (**B**) The percentages of PKH67-positive RBCs in the spleen are represented in bar graph format. (**C**) The experimental design is depicted, wherein C57BL/6 mice (n = 3 per group) were administered a single intravenous dose of Tuftsin (0.15 mg/kg) on days 7 and 11, followed by HH exposure until day 14, culminating in spleen isolation for F4/80 immunohistochemistry and iron staining. (**D**) Demonstrates F4/80 and iron staining in the spleen after 14 days of HH exposure with Tuftsin treatment. (**E**) Quantitative analysis of the relative fluorescence intensity of F4/80 expression in the spleen as described in (**D**). (**F**) Semi-quantitative assessment of iron levels in the spleen as outlined in (**D**). Data presented in this figure are articulated as means ± SEM for each group (n = 3 per group). Statistical significance is denoted by * $P < 0.05$, ** $P < 0.01$, *** $P < 0.001$ when compared to the NN group or as indicated.

Figure 8. HH exposure enhances iron mobilization and induces ferroptosis in the spleen. The C57BL/6 mice were treated with NN and HH for 7 days, and the spleen

was collected for subsequent detection. (**A**) Western blot detection of HO-1, Ft-L, Ft-H, NCOA4, Fpn and TfR protein expression in spleen. (**B**) Statistical analysis of HO-1, Ft-L, Ft-H, NCOA4, Fpn and TfR protein expression. (**C**) GEO data analysis of HMOX1, FTL, FTH1, NCOA4, SLC40A1, and TFRC mRNA expression in PMBCs before and after climbing to HA (n=98). (**D**) Western blot analysis for ACSL4, GPX4, and xCT protein expression in the spleen, with (**E**) depicting the statistical analysis of these protein levels. (**F**) GEO data analysis of ACSL4, GPX4 and SLC7A11 mRNA expression in PMBCs before and after reaching HA (n=98). (**G**) The content of Fe^{2+} in the spleen was detected using the FerroFarRed probe by flow cytometry. (**H**) The level of lipid ROS in the spleen was detected using the C11-BODIPY probe by flow cytometry. The MDA (**I**), Cys (**J**) and GSH (**K**) levels in the spleen were detected using biochemical detection kits, respectively. (**L**) Lillie staining of Fe^{2+} in the spleen after 7 days of HH exposure. (**M**) Fe^{2+} deposition in the spleen as described in (**L**) was quantified. Data are expressed as the means ± SEM (n = 3 per group); * $P < 0.05$, ** $P < 0.01$, *** $P < 0.001$ versus the NN group or the indicated group.

Figure 9. Hypoxia enhances the ferroptosis in splenic macrophage. Splenic macrophages were cultured under 1% hypoxia for varying durations (0, 12, 24, 48 h), either with or without a pre-treatment of 10 μM Fer-1 for 1 h, before being collected for further examination. (**A**) Immunofluorescence detection of Fe^{2+} levels in macrophages after hypoxia exposure for 24 h using the FerroFarRed probe under a

fluorescence microscope. (**B**) Quantitative results of fluorescence intensity in the macrophages described in A. (**C**) Flow cytometry detection of Fe^{2+} levels in macrophages exposed to hypoxia for 24 h using the FerroFarRed probe. (**D**) Immunofluorescence detection of lipid ROS levels in macrophages exposed to hypoxia for 24 h using the C11-BODIPY probe under a fluorescence microscope. (**E**) Quantitative results of mean fluorescence intensity in the macrophages described in (**D**). (**F**) Western blot detection of ACSL4, GPX4 and xCT protein expression in macrophages under hypoxia for different times. (**G**) Flow cytometry was employed to analyze Calcein/PI double staining in macrophages following a 24 h hypoxia exposure. (**H**) Cell death proportions in macrophages are given as bar graphs. (**I**) Macrophage phagocytic activity against Cy5.5-labelled *E.coli* following 24 h of hypoxia exposure was assessed using flow cytometry *in vitro*. (**J**) Fe^{2+} levels in macrophages pre-treated with Fer-1, then exposed to 24 h of hypoxia, were detected via the FerroFarRed probe in immunofluorescence. (**K**) Quantitative results of fluorescence intensity in the macrophages described in (**J**). (**L**) Western blot detection of ACSL4, GPX4 and xCT protein expression in macrophages pre-treated with Fer-1, then followed by 24 h of hypoxia exposure. (**M-O**) Statistical analysis of ACSL4, xCT, and GPX4 protein expression in L. MDA (**P**), Cys (**Q**), and GSH (**R**) levels in macrophages pre-treated with Fer-1 and subsequently exposed to 24 h of hypoxia were detected using kits and biochemical methods. Data are expressed as the means ± SEM (n = 3 per group); * $P < 0.05$, ** $P < 0.01$, *** $P < 0.001$ versus the NN group or the indicated group.

Figure 10. HA/HH exposure suppresses erythrophagocytosis by inducing macrophages ferroptosis in the spleen. This figure summarizes the multifaceted impact of HA and HH exposure on splenic macrophage function. HA/HH exposure is demonstrated to trigger significant iron mobilization, notably increasing Fe^{2+} levels, which are further elevated in the spleen and macrophages of mice. Concurrently, HA/HH exposure is associated with an upregulation of ACSL4 expression, coupled with a suppression of xCT expression and GSH production. This alteration results in enhanced lipid peroxidation, culminating in the escalation of macrophage ferroptosis. Additionally, the exposure adversely affects monocyte migration and differentiation from BM to the spleen. Collectively, these effects of HA/HH exposure contribute to a notable inhibition of erythrophagocytosis, thereby promoting erythrocytosis and potentially exacerbating the progression of HAPC. This comprehensive analysis underscores the intricate interplay between environmental factors and cellular mechanisms in the spleen, which could significantly influence the pathogenesis of HAPC.

Supplementary Figure S1. HH exposure induces RPMs reduction in the spleen. (**A**) Immunofluorescence techniques were utilized to concurrently detect F4/80 and CD11b, and (**C**) F4/80 and CD68, to identify RPM contents in the spleen post-perfusion at 7 and 14 days of HH exposure. (**B** and **D**) Quantitative analyses of $F4/80^{hi}CD11b^{lo}$ and $F4/80^{hi}CD68^{hi}$ cell populations in the spleen, as described in (**A**

and **C**), were conducted. Data presented in this figure are expressed as means ±SEM for each group (n = 3 per group). Statistical significance is indicated by * $P < 0.05$, *** $P < 0.001$ when compared to the NN group or as indicated. The results demonstrate a significant reduction in RPMs in the spleen following HH exposure, highlighting the effects of hypoxic conditions on splenic macrophage populations.

Supplementary Figure S2. HH exposure induces transformation of RPMs subsets in the spleen. This figure presents the analysis of RPMs in the spleen following 7 days of HH exposure, utilizing single-cell sequencing. (**A**) Marker genes were employed to identify RPMs within splenic cells, referencing Cell Marker 2.0. (**B**) RPMs in the spleen were categorized into three distinct clusters (0, 1, and 2) based on their gene expression profiles post-HH exposure. (**C**) Presenting the characteristic gene expression associated with each of these clusters in RPMs. (**D**) Pseudotime analysis of RPMs in the spleen was performed, with the trajectory figure illustrating the developmental pathway of these cells. This analysis elucidates the intricate changes in RPM subpopulations in the spleen under HH conditions, providing insights into the cellular dynamics and transcriptional alterations in response to hypoxia.

Supplementary Figure S3. HH exposure promotes iron mobilization and induces ferroptosis in the spleen. The C57BL/6 mice were treated with NN and HH for 14 days, and the spleen was collected for subsequent detection. (**A**) Western blot analysis

was conducted to assess the expression levels of HO-1, Ft-L, Ft-H, NCOA4, Fpn, and TfR proteins in the spleen. (**B**) Statistical analysis of the protein expression levels detailed in (**A**). (**C**) Western blot analysis for ACSL4, GPX4, and xCT protein expression in the spleen. (**D**) The statistical analysis of these protein expression as shown in (**C**). (**E**) Flow cytometry using the FerroFarRed probe was employed to detect Fe^{2+} content in the spleen. (**F**) Quantitative results of the mean fluorescence intensity from (**E**). (**G**) Lipid ROS levels in the spleen were measured using the C11-BODIPY probe and flow cytometry. (**H**) Quantification of mean fluorescence intensity from (**G**). Levels of MDA (**I**), Cys (**J**), and GSH (**K**) in the spleen were determined using specific biochemical detection kits. (**L**) Lillie staining was performed to visualize Fe^{2+} in the spleen post 14-day HH exposure, with (**M**) providing a quantification of Fe^{2+} deposition as depicted in (**L**). Data are expressed as means ± SEM for each group (n = 3 per group). Statistical significance is denoted by * $P < 0.05$, ** $P < 0.01$, *** $P < 0.001$ when compared to the NN group or as indicated. These results collectively emphasize the significant impact of HH on the iron metabolism in the spleen, particularly highlighting the increased mobilization of iron and the onset of ferroptosis under hypoxic conditions.

Figure 1

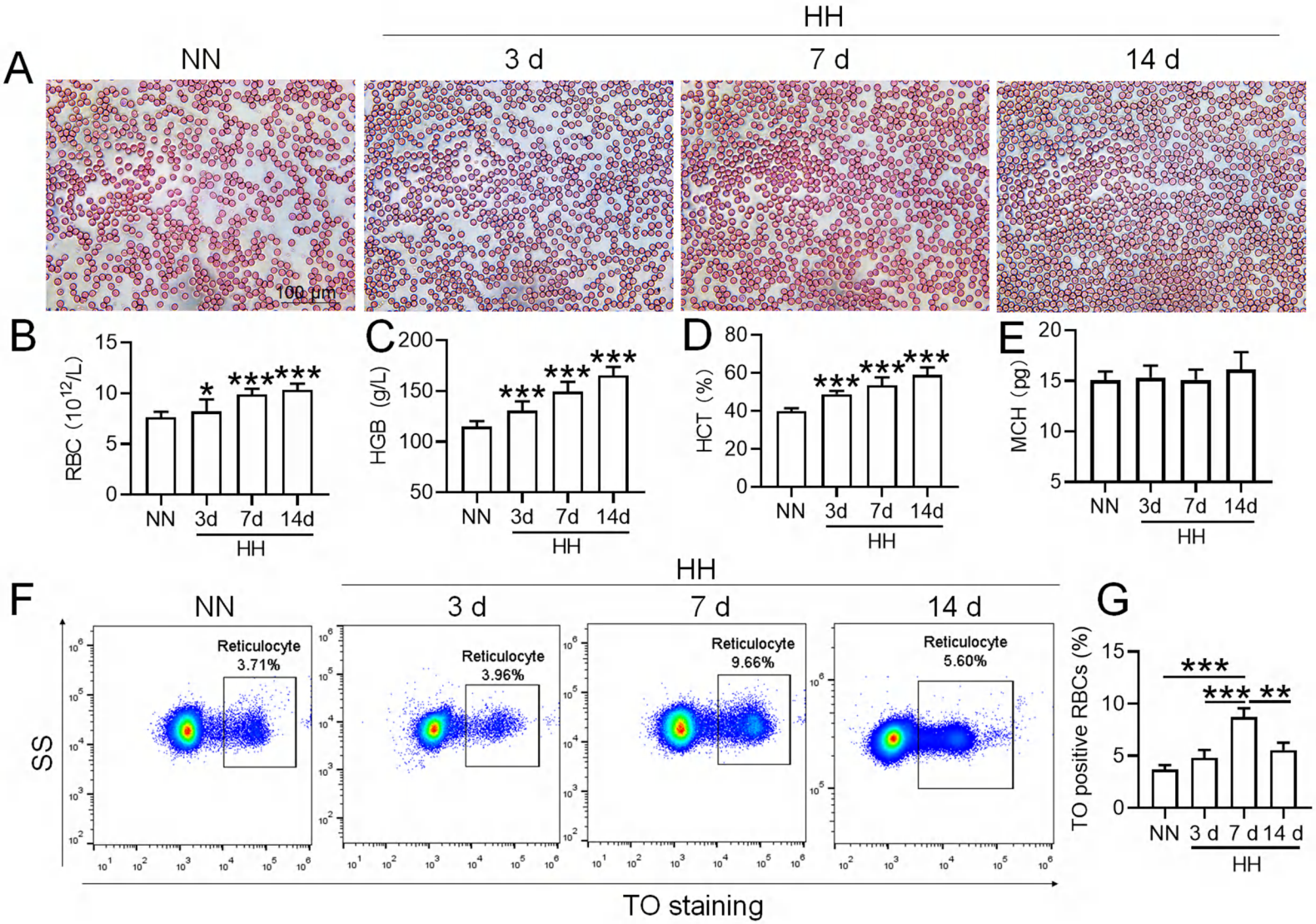
A
NN
HH
3 d
7 d
14 d
100 μm
B
RBC (10^12/L)
C
HGB (g/L)
D
HCT (%)
E
MCH (pg)
NN
3d
7d
14d
HH
F
Reticulocyte 3.71%
Reticulocyte 3.96%
Reticulocyte 9.66%
Reticulocyte 5.60%
SS
TO staining
G
TO positive RBCs (%)

Figure 2

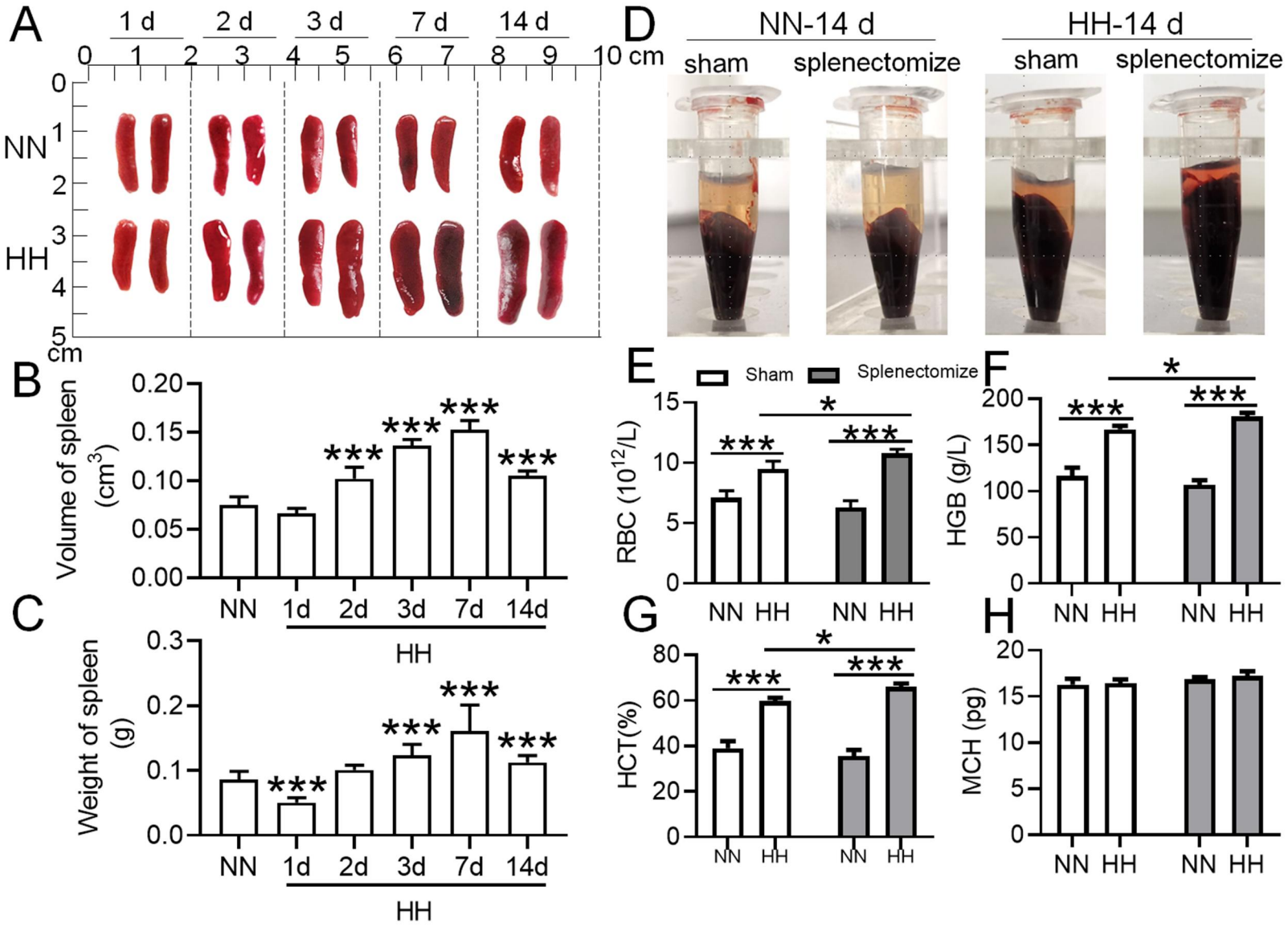
A
1 d
2 d
3 d
7 d
14 d
0 1 2 3 4 5 6 7 8 9 10 cm
NN
HH
cm
B
Volume of spleen (cm3)
0.20
0.15
0.10
0.05
0.00
***
NN 1d 2d 3d 7d 14d
HH
C
Weight of spleen (g)
0.3
0.2
0.1
0.0
***
NN 1d 2d 3d 7d 14d
HH
D
NN-14 d
HH-14 d
sham
splenectomize
sham
splenectomize
E
Sham
Splenectomize
RBC (10^12/L)
15
10
5
0
*
***
NN HH NN HH
F
HGB (g/L)
200
150
100
50
0
*
***
NN HH NN HH
G
HCT(%)
80
60
40
20
0
*
***
NN HH NN HH
H
MCH (pg)
20
15
10
5
0
NN HH NN HH

Figure 3

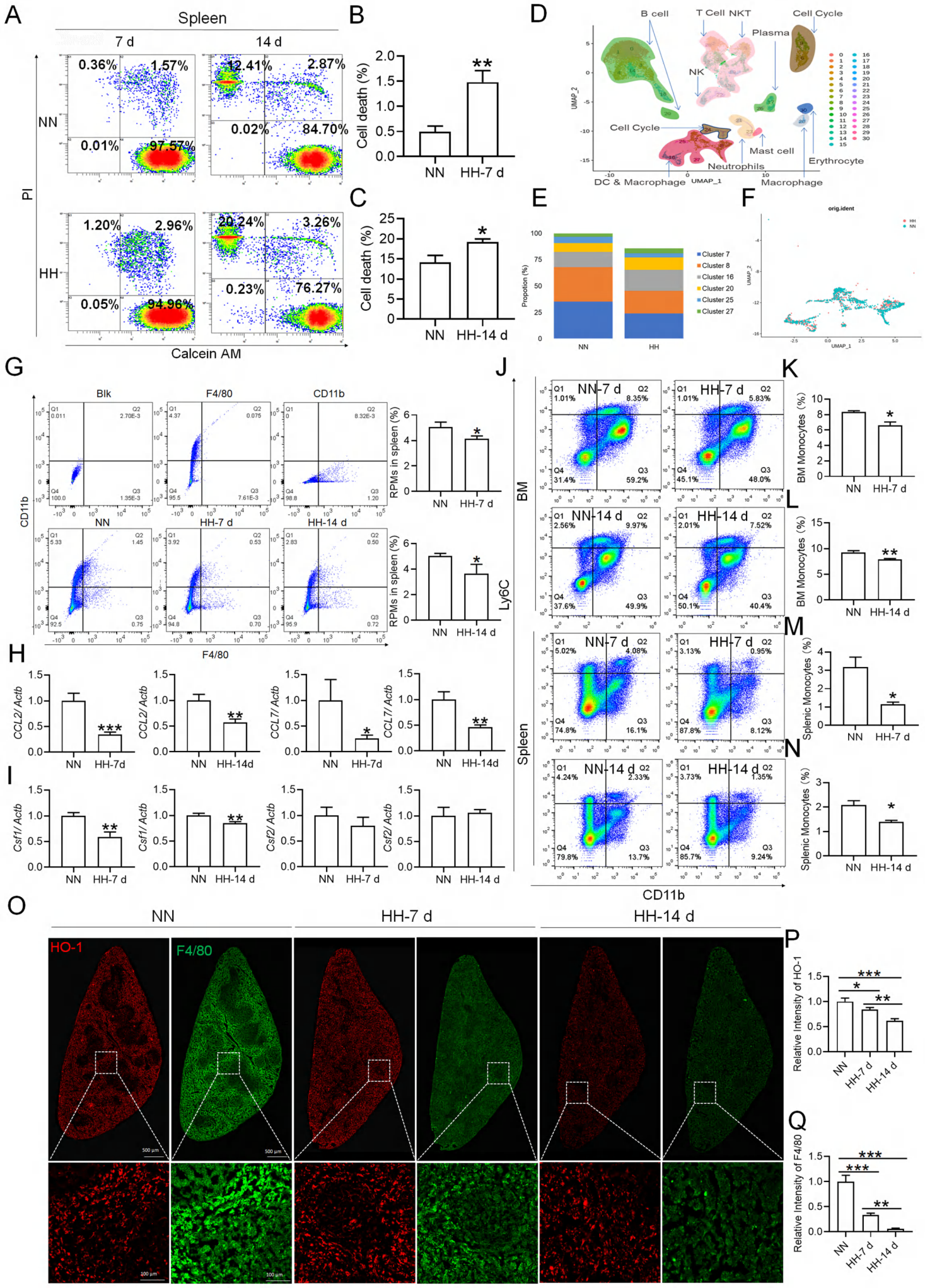
A
Spleen
7 d
14 d
NN
HH
PI
Calcein AM
0.36%
1.57%
0.01%
97.57%
12.41%
2.87%
0.02%
84.70%
1.20%
2.96%
0.05%
94.96%
20.24%
3.26%
0.23%
76.27%
B
Cell death (%)
NN
HH-7 d
C
HH-14 d
D
B cell
T Cell NKT
Cell Cycle
Plasma
NK
Mast cell
Erythrocyte
Neutrophils
DC & Macrophage
Macrophage
UMAP_1
UMAP_2
E
Propotion (%)
Cluster 7
Cluster 8
Cluster 16
Cluster 20
Cluster 25
Cluster 27
F
orig.ident
HH
NN
G
Blk
F4/80
CD11b
RPMs in spleen (%)
H
CCL2/ Actb
CCL7/ Actb
I
Csf1/ Actb
Csf2/ Actb
J
BM
Spleen
Ly6C
NN-7 d
HH-7 d
NN-14 d
HH-14 d
K
BM Monocytes (%)
L
M
Splenic Monocytes (%)
N
O
HO-1
F4/80
P
Relative Intensity of HO-1
Q
Relative Intensity of F4/80

Figure 4

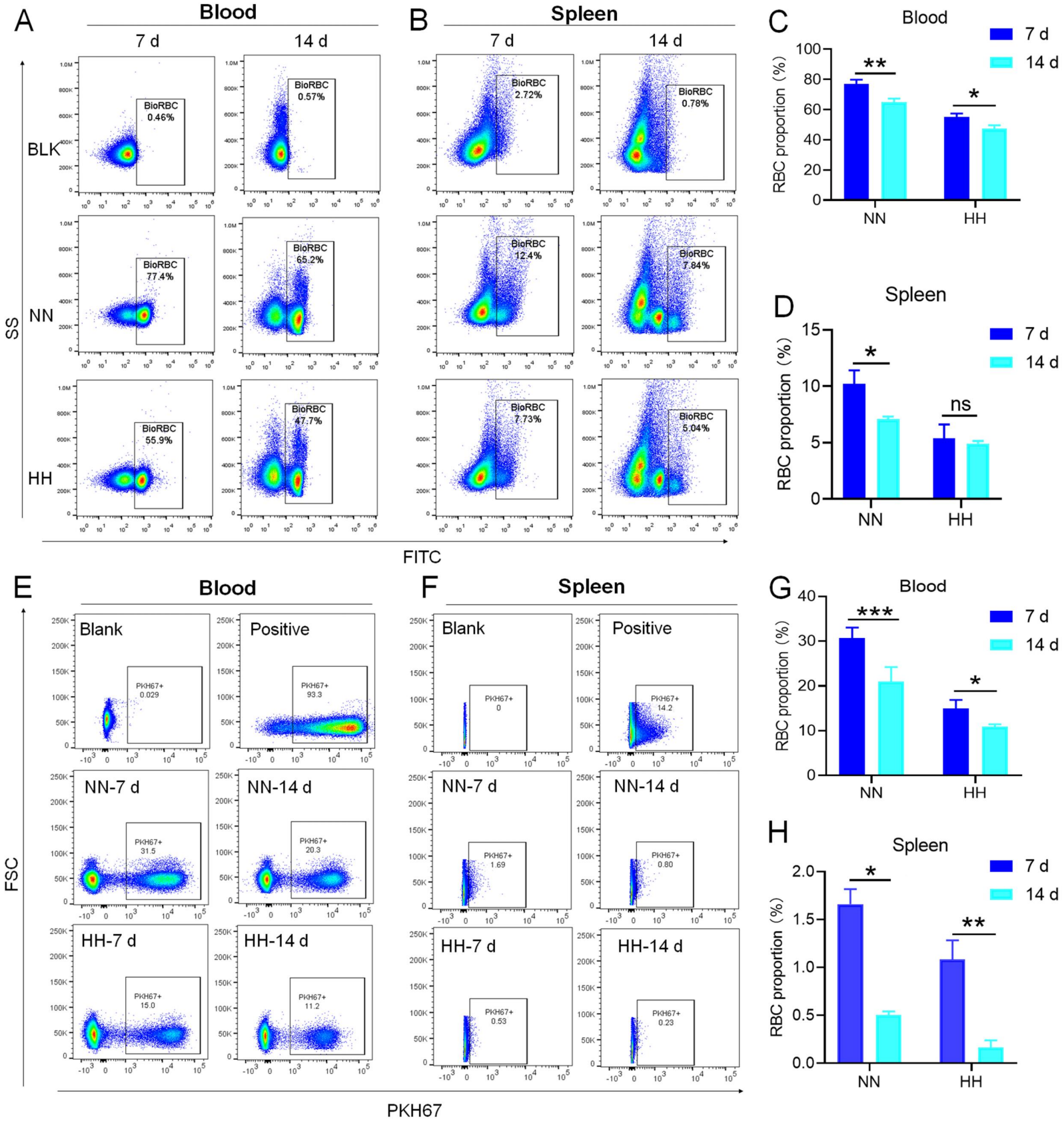
A
Blood
7 d
14 d
BLK
NN
HH
BioRBC 0.46%
BioRBC 0.57%
BioRBC 77.4%
BioRBC 65.2%
BioRBC 55.9%
BioRBC 47.7%
SS
FITC
B
Spleen
BioRBC 2.72%
BioRBC 0.78%
BioRBC 12.4%
BioRBC 7.84%
BioRBC 7.73%
BioRBC 5.04%
C
Blood
7 d
14 d
RBC proportion (%)
NN
HH
D
Spleen
ns
E
Blank
Positive
NN-7 d
NN-14 d
HH-7 d
HH-14 d
PKH67+ 0.029
PKH67+ 93.3
PKH67+ 31.5
PKH67+ 20.3
PKH67+ 15.0
PKH67+ 11.2
FSC
PKH67
F
PKH67+ 0
PKH67+ 14.2
PKH67+ 1.69
PKH67+ 0.80
PKH67+ 0.53
PKH67+ 0.23
G
H

Figure 5

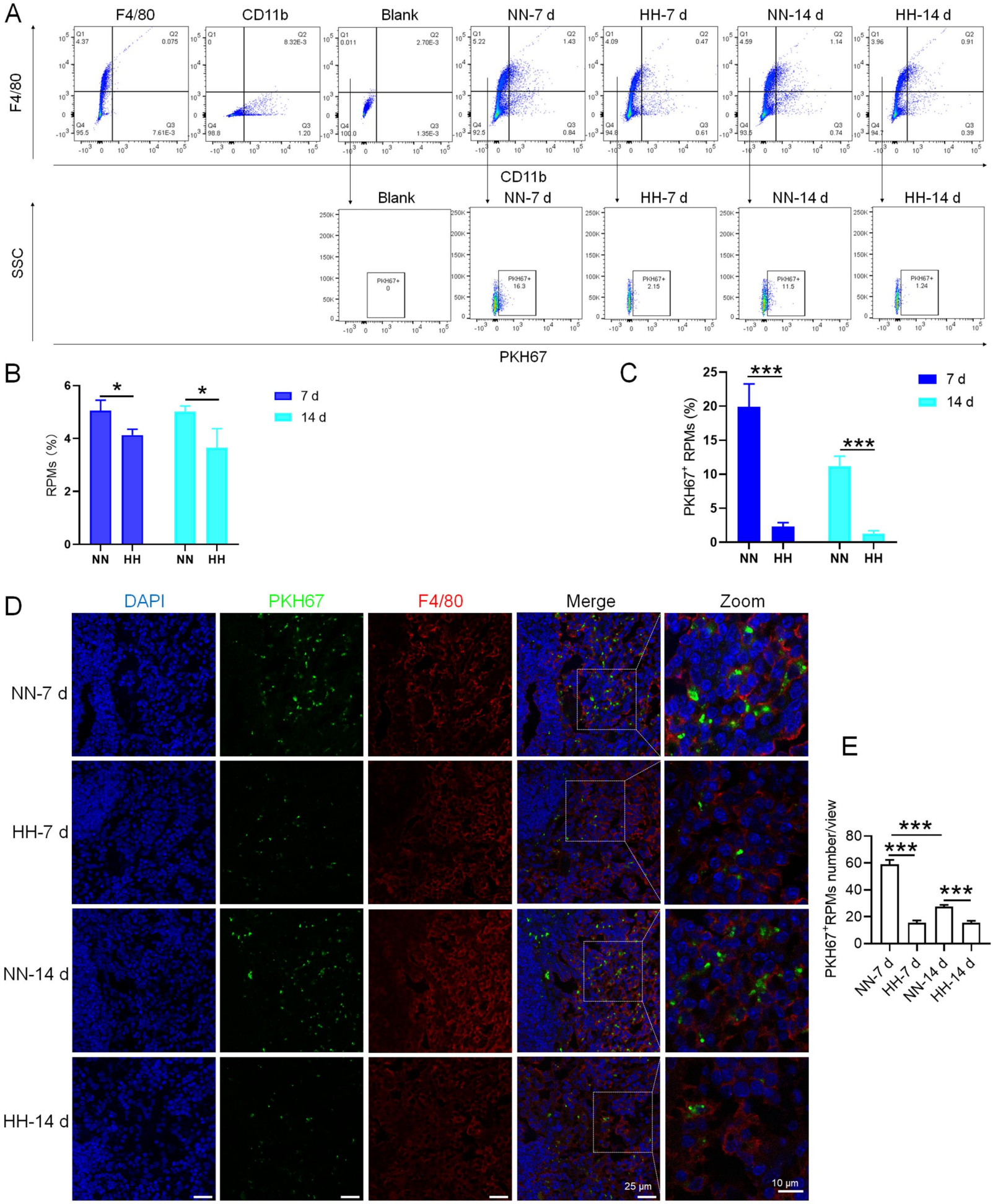
A
F4/80
CD11b
Blank
NN-7 d
HH-7 d
NN-14 d
HH-14 d
SSC
PKH67
B
RPMs (%)
7 d
14 d
NN
HH
C
PKH67+ RPMs (%)
D
DAPI
PKH67
F4/80
Merge
Zoom
25 μm
10 μm
E
PKH67+RPMs number/view

Figure 6

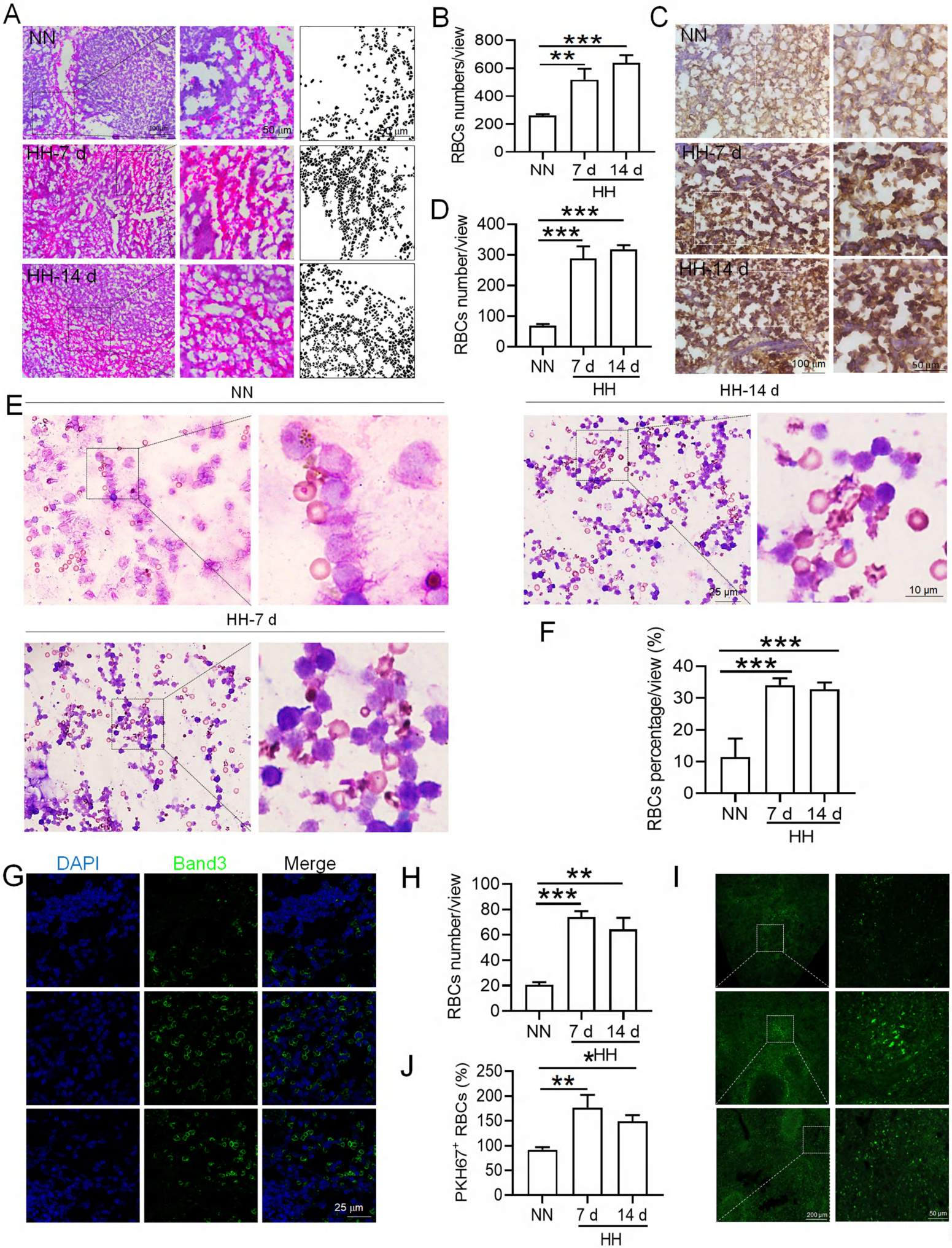
A
NN
HH-7 d
HH-14 d
100 μm
50 μm
B
RBCs numbers/view
800
600
400
200
0
***
**
NN
7 d
14 d
HH
C
NN
HH-7 d
HH-14 d
100 μm
50 μm
D
RBCs number/view
400
300
200
100
0
***
***
NN
7 d
14 d
HH
E
NN
HH-7 d
HH-14 d
25 μm
10 μm
F
RBCs percentage/view (%)
40
30
20
10
0
***
***
NN
7 d
14 d
HH
G
DAPI
Band3
Merge
25 μm
H
RBCs number/view
100
80
60
40
20
0
**
***
NN
7 d
14 d
*HH
I
200 μm
50 μm
J
PKH67+ RBCs (%)
250
200
150
100
50
0
**
NN
7 d
14 d
HH

Figure 7

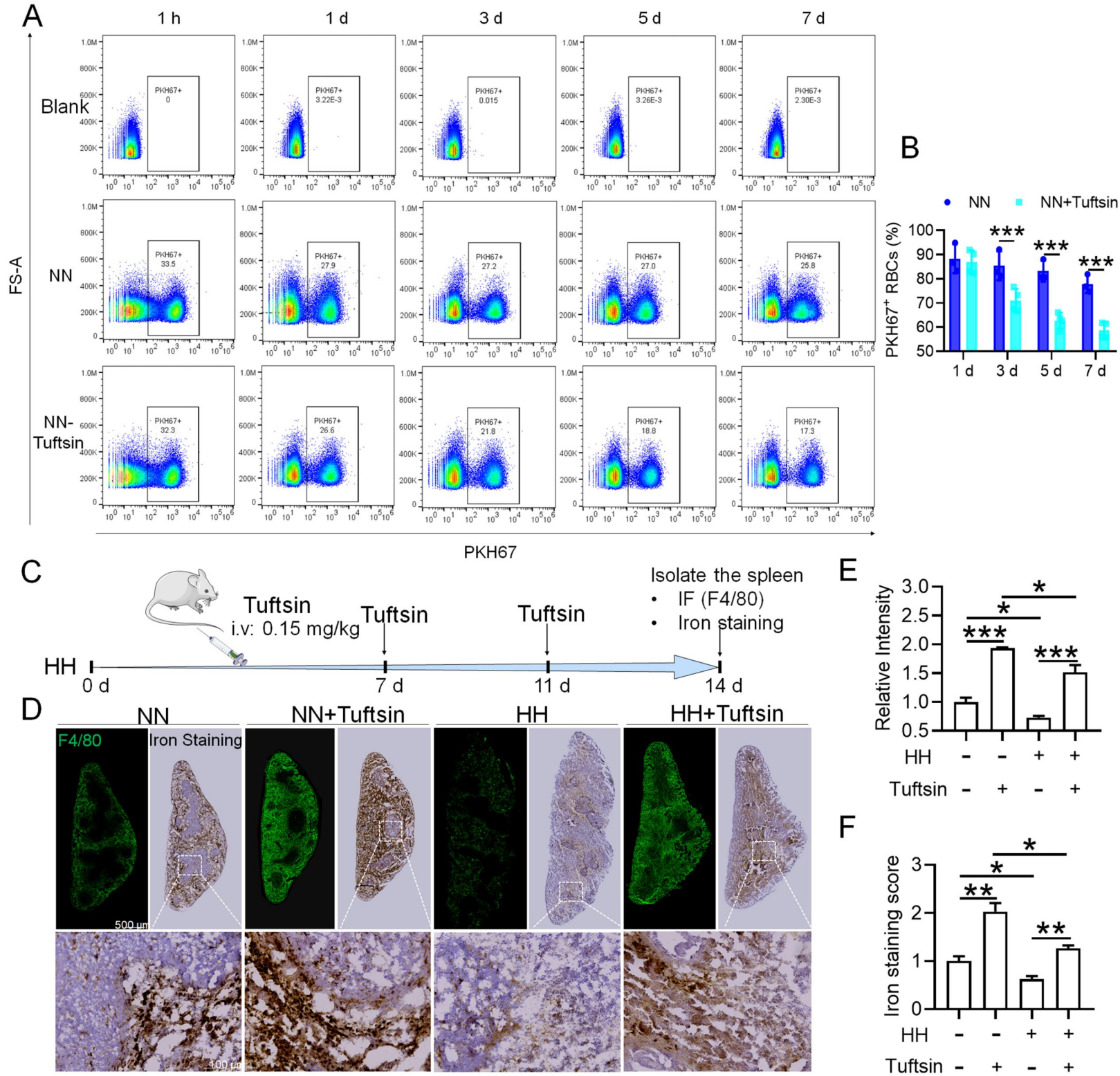
A
1 h
1 d
3 d
5 d
7 d
Blank
NN
NN-Tuftsin
FS-A
PKH67
PKH67+ 0
PKH67+ 3.22E-3
PKH67+ 0.015
PKH67+ 3.26E-3
PKH67+ 2.30E-3
PKH67+ 33.5
PKH67+ 27.9
PKH67+ 27.2
PKH67+ 27.0
PKH67+ 25.8
PKH67+ 32.3
PKH67+ 26.6
PKH67+ 21.8
PKH67+ 18.8
PKH67+ 17.3
B
NN
NN+Tuftsin
PKH67+ RBCs (%)
1 d
3 d
5 d
7 d
C
Tuftsin
i.v: 0.15 mg/kg
Tuftsin
Tuftsin
Isolate the spleen
IF (F4/80)
Iron staining
HH
0 d
7 d
11 d
14 d
D
NN
NN+Tuftsin
HH
HH+Tuftsin
F4/80
Iron Staining
E
Relative Intensity
HH
Tuftsin
F
Iron staining score
HH
Tuftsin

Figure 8

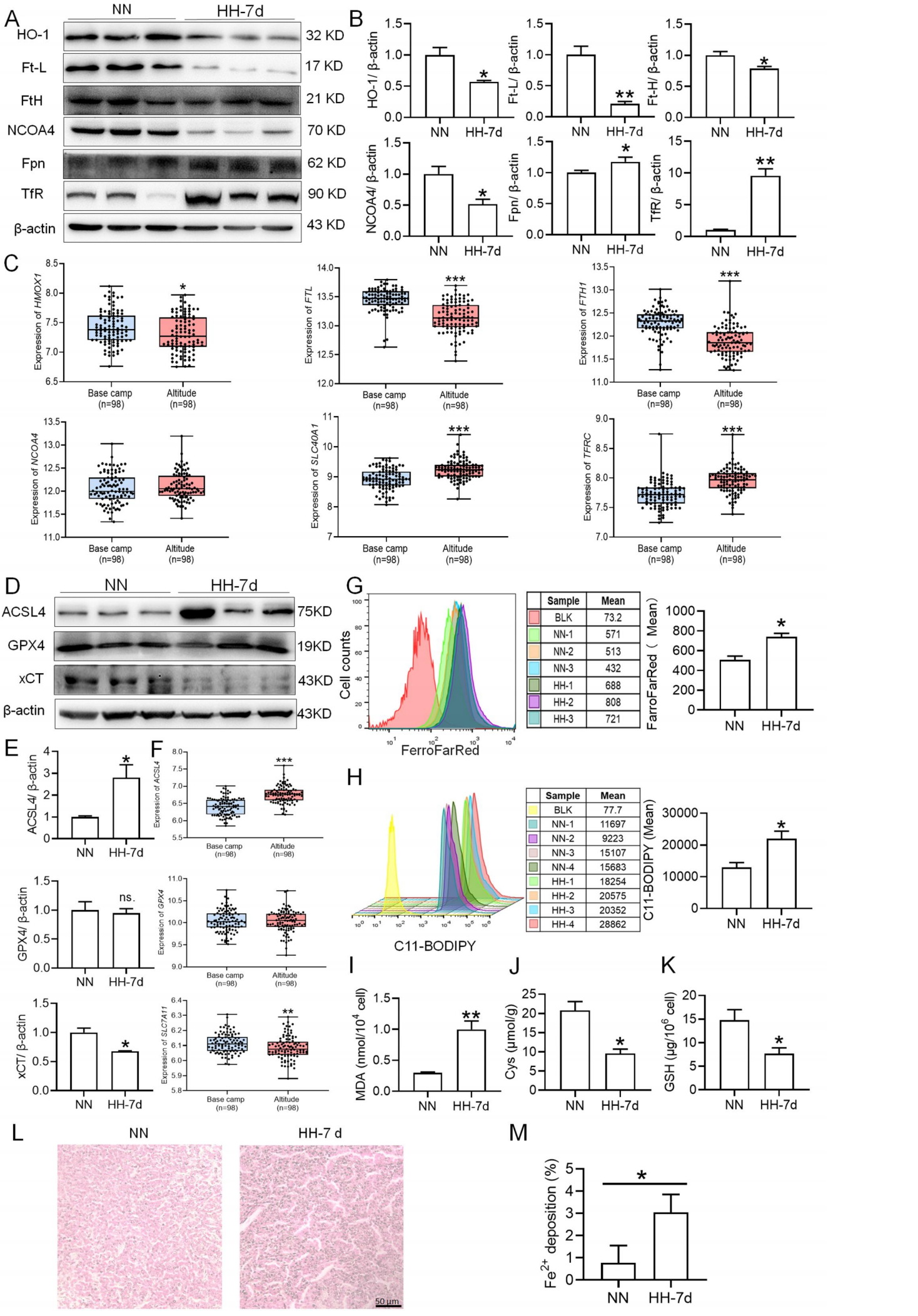
A
NN
HH-7d
HO-1
Ft-L
FtH
NCOA4
Fpn
TfR
β-actin
32 KD
17 KD
21 KD
70 KD
62 KD
90 KD
43 KD
B
HO-1/ β-actin
Ft-L/ β-actin
Ft-H/ β-actin
NCOA4/ β-actin
Fpn/ β-actin
TfR/ β-actin
C
Expression of HMOX1
Expression of FTL
Expression of FTH1
Expression of NCOA4
Expression of SLC40A1
Expression of TFRC
Base camp (n=98)
Altitude (n=98)
D
ACSL4
GPX4
xCT
β-actin
75KD
19KD
43KD
43KD
E
ACSL4/ β-actin
GPX4/ β-actin
xCT/ β-actin
ns.
F
Expression of ACSL4
Expression of GPX4
Expression of SLC7A11
G
Cell counts
FerroFarRed
Sample | Mean
BLK | 73.2
NN-1 | 571
NN-2 | 513
NN-3 | 432
HH-1 | 688
HH-2 | 808
HH-3 | 721
FarroFarRed（Mean）
H
C11-BODIPY
Sample | Mean
BLK | 77.7
NN-1 | 11697
NN-2 | 9223
NN-3 | 15107
NN-4 | 15683
HH-1 | 18254
HH-2 | 20575
HH-3 | 20352
HH-4 | 28862
C11-BODIPY (Mean)
I
MDA (nmol/10^4 cell)
J
Cys (μmol/g)
K
GSH (μg/10^6 cell)
L
NN
HH-7 d
50 μm
M
Fe^2+ deposition (%)

Figure 9

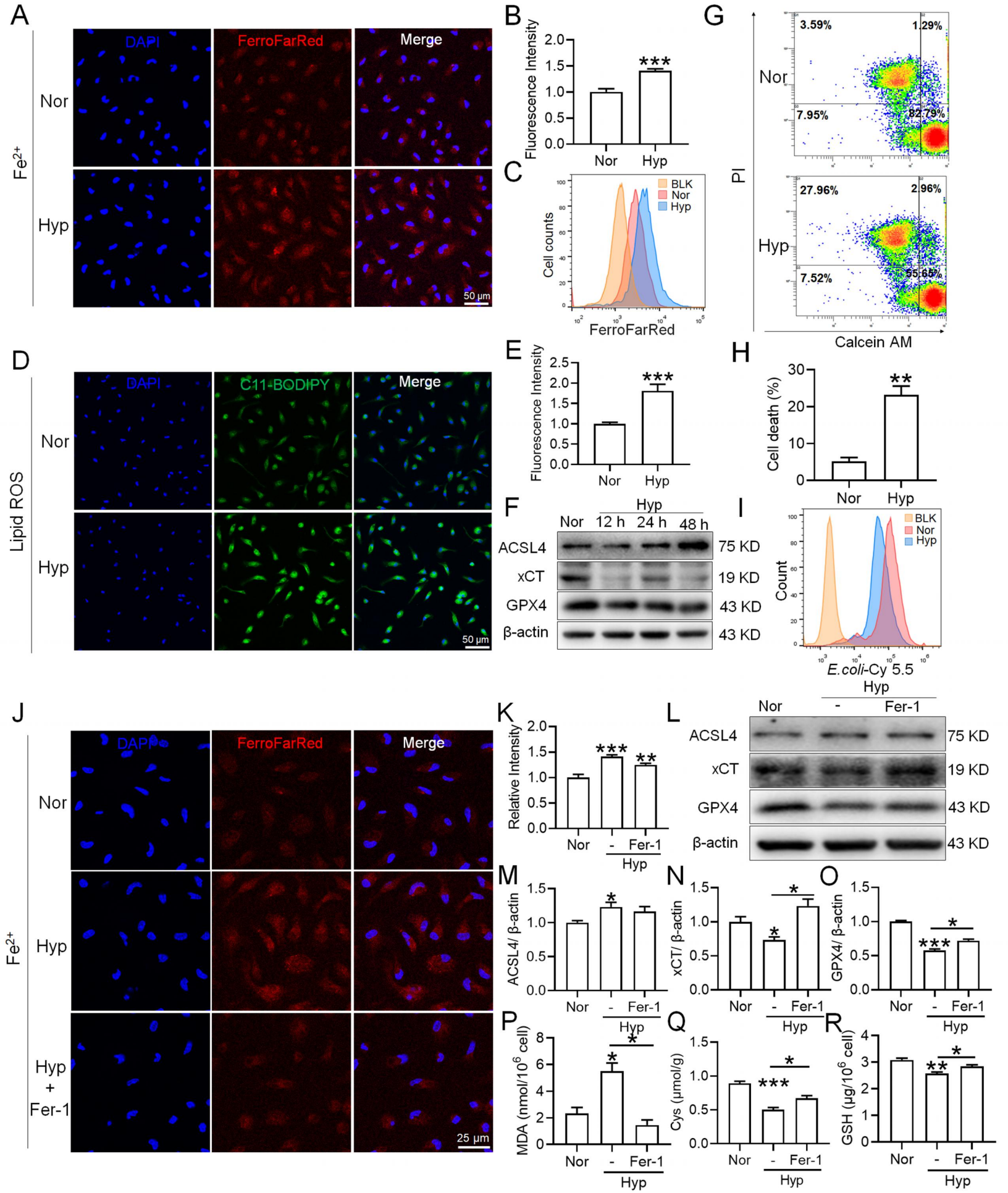
A
DAPI
FerroFarRed
Merge
Nor
Hyp
Fe2+
50 μm
B
Fluorescence Intensity
***
Nor
Hyp
C
BLK
Nor
Hyp
Cell counts
FerroFarRed
G
3.59%
1.29%
7.95%
82.79%
27.96%
2.96%
7.52%
55.65%
PI
Calcein AM
D
DAPI
C11-BODIPY
Merge
Lipid ROS
50 μm
E
Fluorescence Intensity
***
H
Cell death (%)
**
F
Hyp
12 h
24 h
48 h
ACSL4
xCT
GPX4
β-actin
75 KD
19 KD
43 KD
43 KD
I
BLK
Nor
Hyp
Count
E.coli-Cy 5.5
J
DAPI
FerroFarRed
Merge
Hyp + Fer-1
25 μm
K
Relative Intensity
***
**
Fer-1
L
ACSL4/ β-actin
xCT/ β-actin
GPX4/ β-actin
M
N
O
P
MDA (nmol/10^6 cell)
Q
Cys (μmol/g)
R
GSH (μg/10^6 cell)

Figure 10

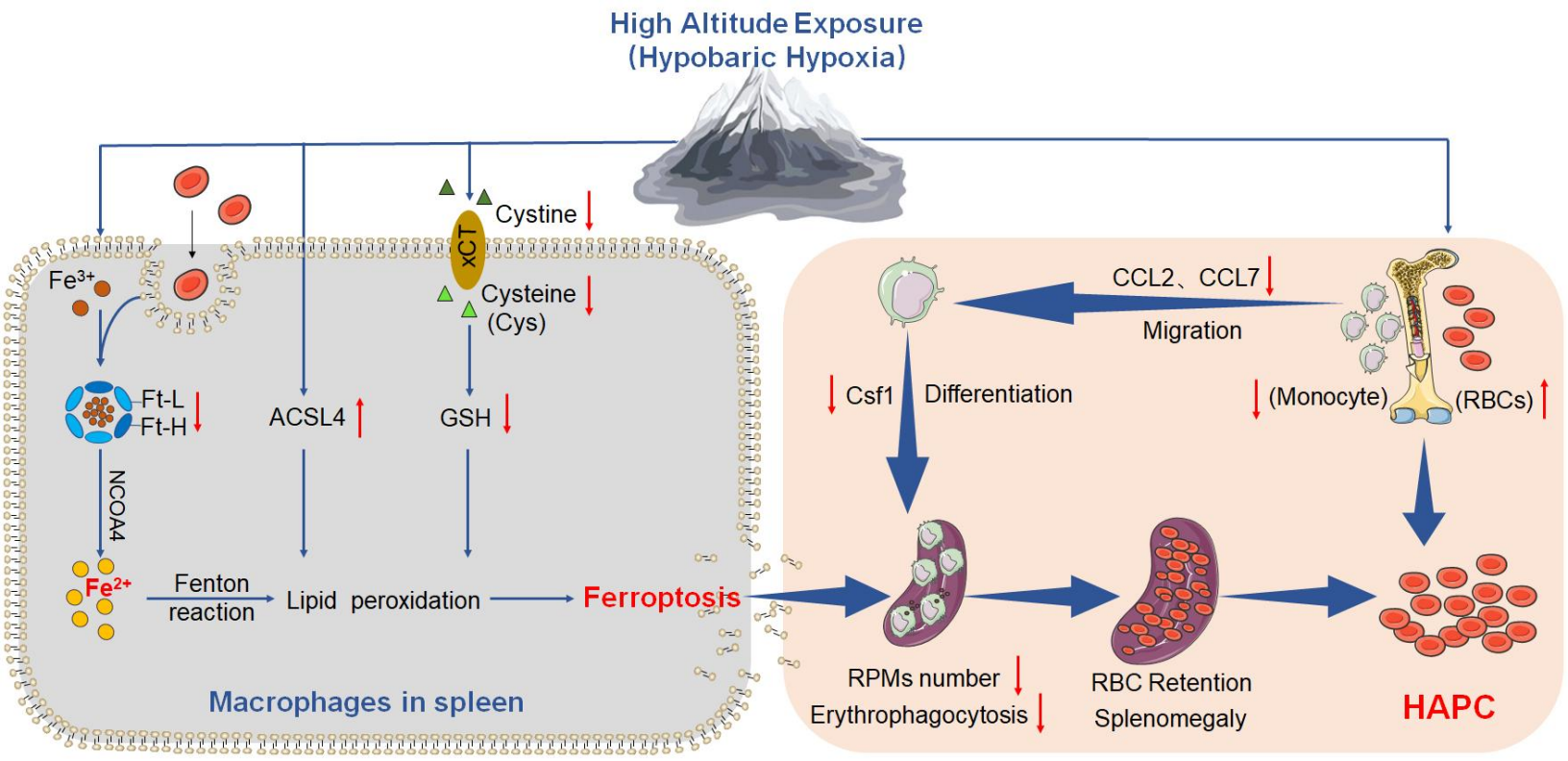
High Altitude Exposure
(Hypobaric Hypoxia)
Cystine
xCT
Cysteine
(Cys)
Fe3+
Ft-L
Ft-H
ACSL4
GSH
NCOA4
Fe2+
Fenton
reaction
Lipid peroxidation
Ferroptosis
Macrophages in spleen
CCL2、CCL7
Migration
Csf1
Differentiation
(Monocyte)
(RBCs)
RPMs number
Erythrophagocytosis
RBC Retention
Splenomegaly
HAPC

Figure S1

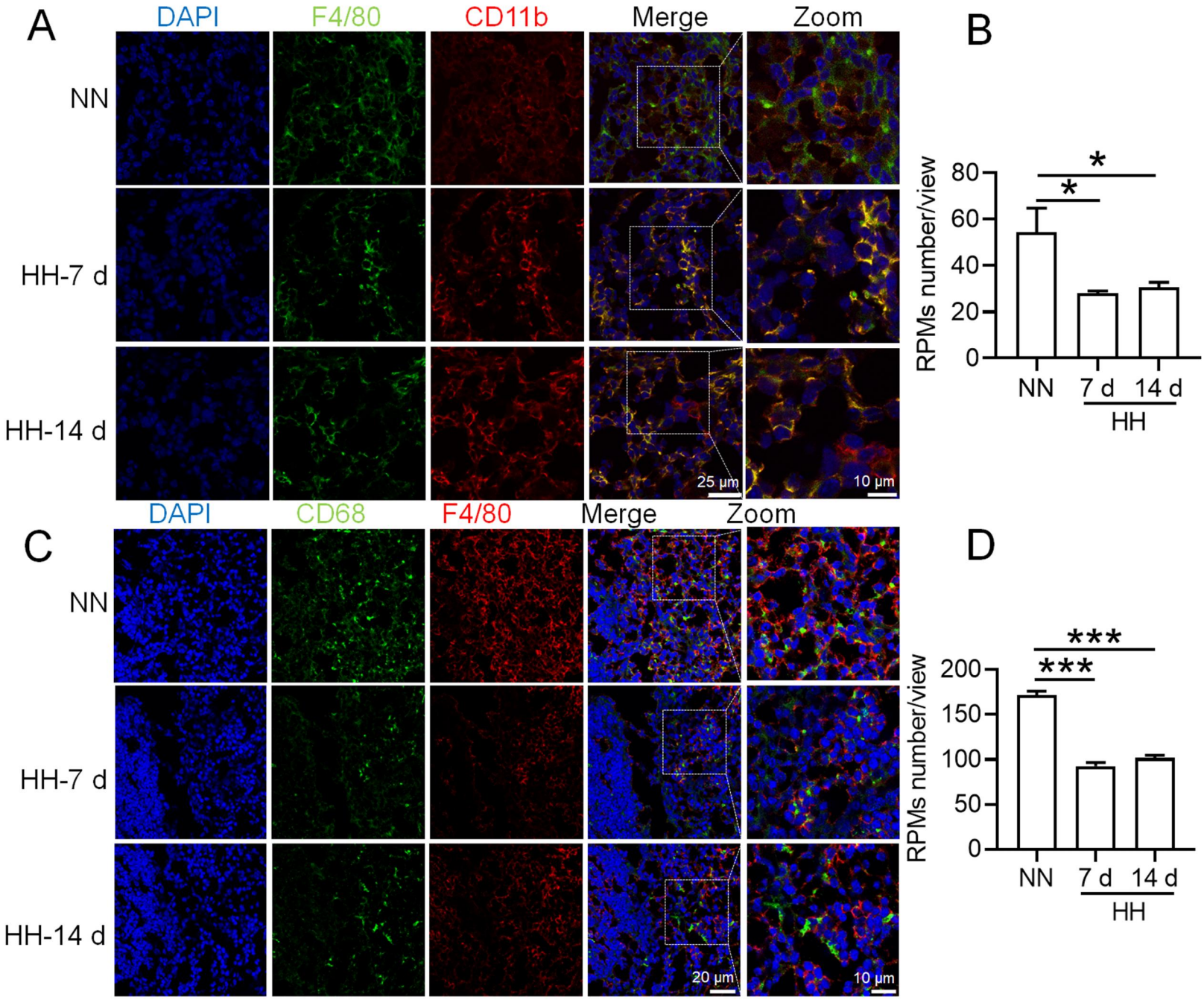
A
DAPI
F4/80
CD11b
Merge
Zoom
NN
HH-7 d
HH-14 d
25 μm
10 μm
B
RPMs number/view
80
60
40
20
0
*
*
NN
7 d
14 d
HH
C
DAPI
CD68
F4/80
Merge
Zoom
NN
HH-7 d
HH-14 d
20 μm
10 μm
D
RPMs number/view
200
150
100
50
0
***
***
NN
7 d
14 d
HH

Figure S2

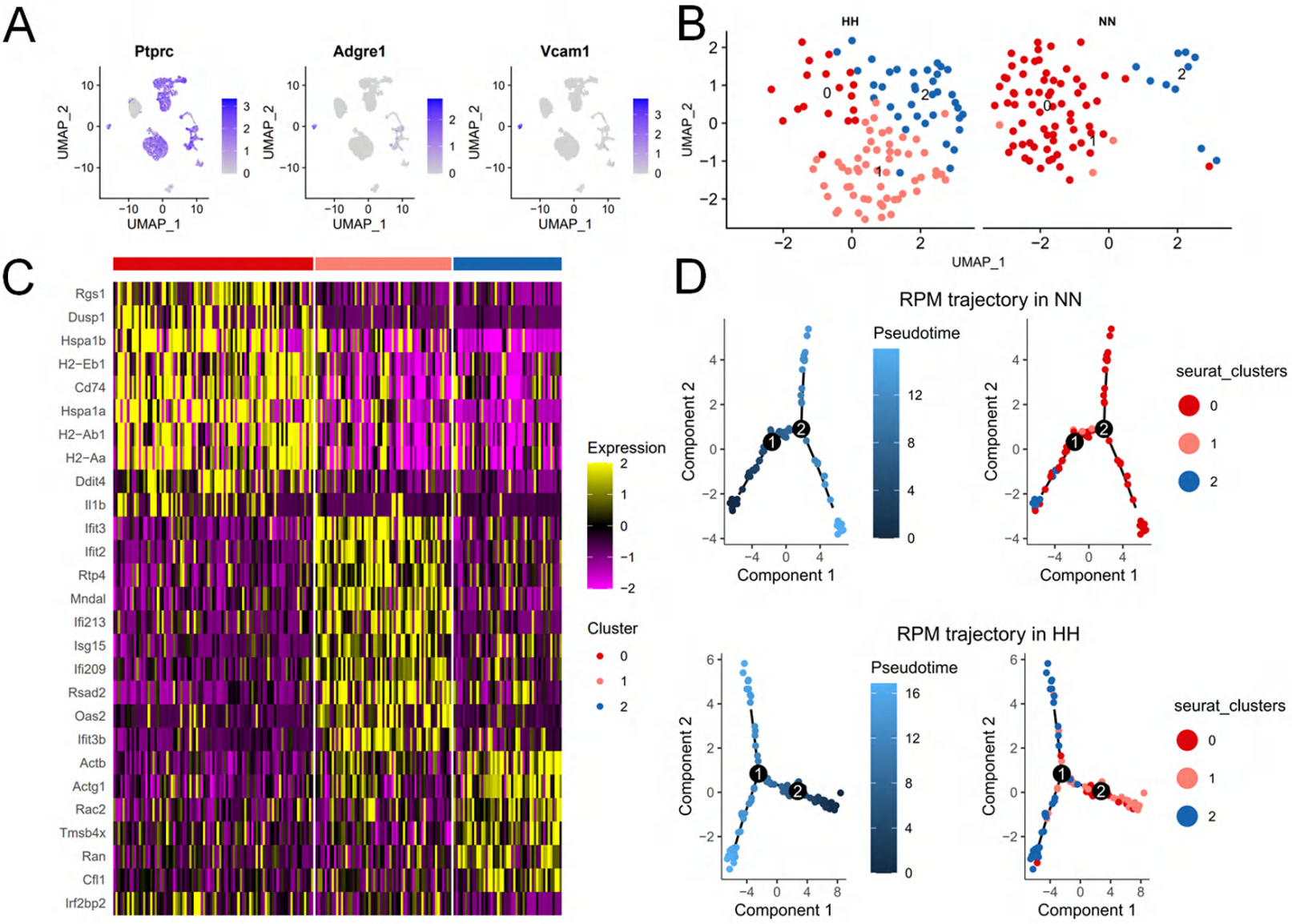
A
Ptprc
Adgre1
Vcam1
UMAP_1
UMAP_2
B
HH
NN
UMAP_1
UMAP_2
C
Rgs1
Dusp1
Hspa1b
H2−Eb1
Cd74
Hspa1a
H2−Ab1
H2−Aa
Ddit4
Il1b
Ifit3
Ifit2
Rtp4
Mndal
Ifi213
Isg15
Ifi209
Rsad2
Oas2
Ifit3b
Actb
Actg1
Rac2
Tmsb4x
Ran
Cfl1
Irf2bp2
Expression
Cluster
D
RPM trajectory in NN
Pseudotime
seurat_clusters
Component 1
Component 2
RPM trajectory in HH

Figure S3

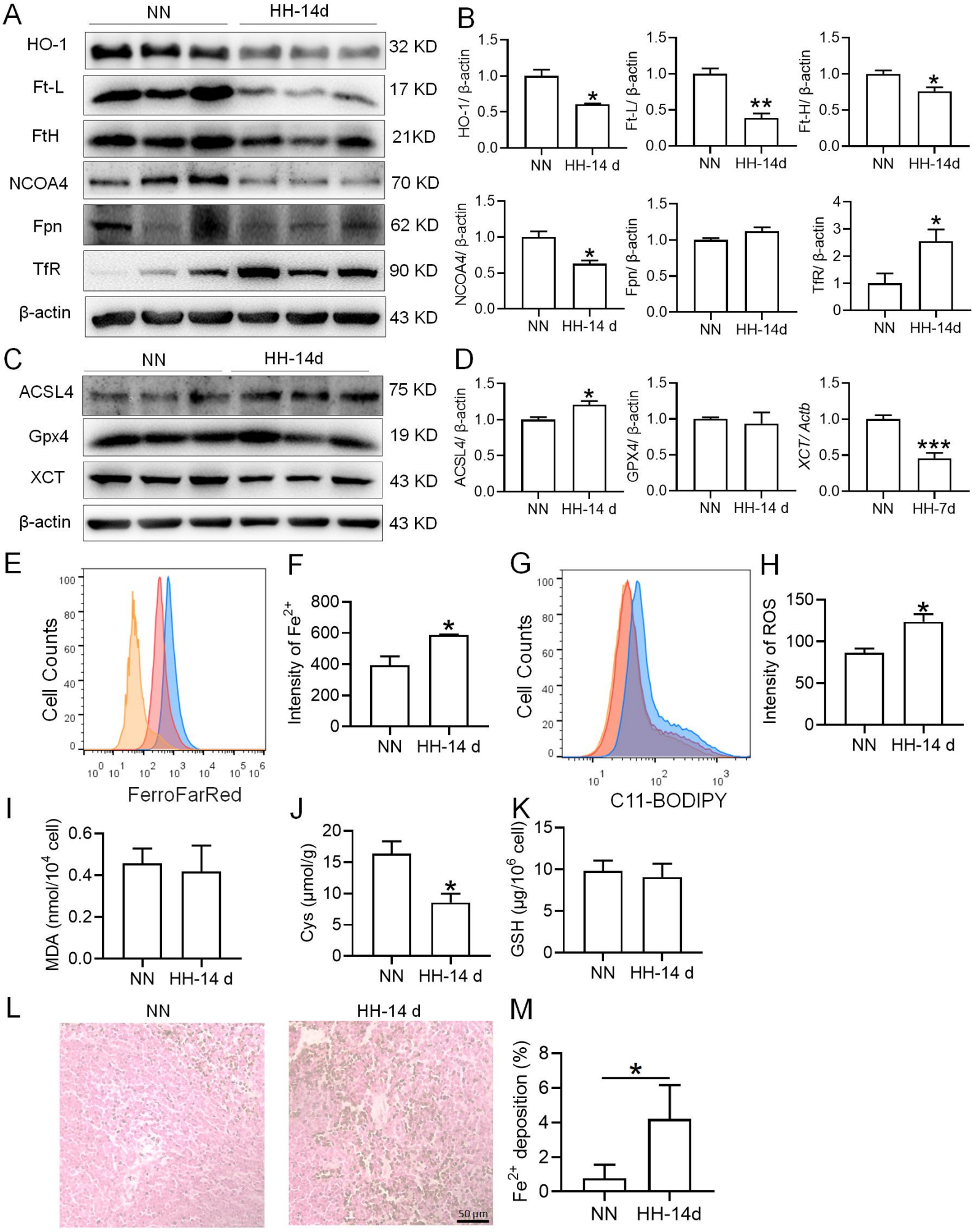
A
NN
HH-14d
HO-1
Ft-L
FtH
NCOA4
Fpn
TfR
β-actin
32 KD
17 KD
21KD
70 KD
62 KD
90 KD
43 KD
B
HO-1/ β-actin
Ft-L/ β-actin
Ft-H/ β-actin
NCOA4/ β-actin
Fpn/ β-actin
TfR/ β-actin
NN
HH-14 d
HH-14d
C
ACSL4
Gpx4
XCT
β-actin
75 KD
19 KD
43 KD
43 KD
D
ACSL4/ β-actin
GPX4/ β-actin
XCT/ Actb
HH-7d
E
Cell Counts
FerroFarRed
F
Intensity of Fe2+
G
Cell Counts
C11-BODIPY
H
Intensity of ROS
I
MDA (nmol/104 cell)
J
Cys (μmol/g)
K
GSH (μg/106 cell)
L
50 μm
M
Fe2+ deposition (%)